NAM

High resolution InSAR in the Groningen area

2018-2019 Advanced Services

SkyGeo: Yuxiao Qin, Jacqueline Salzer, Hanno Maljaars and Pieter Bas Leezenberg

Datum November 2019

Editors Jan van Elk & Dirk Doornhof

General Introduction

Gas production and the resulting reduction of reservoir pressure cause compaction of the reservoir formation. This is expressed as subsidence at surface, which e.g. requires measures to maintain the ground water level in the area above the Groningen gas field. Subsidence measurements are also used to determine the compaction of the gas reservoir, which drives seismicity in the Groningen area. Monitoring of subsidence is therefore an important activity for NAM. Different techniques are used to monitor subsidence: levelling surveys, GPS-measurements and InSAR satellite observations.

Additionally, InSAR offers the opportunity to monitor movement and deformation of infrastructure and larger buildings.

This report describes processing of high-resolution radar image data. In the Study and Data Acquisition Plan (ref. 1 and 2) the objectives of the project were set:

1. Building deformation monitoring;
2. Continuous improvement of InSAR processing and value-adding analysis approaches;
3. Development of visualization tools and establishing an InSAR deliverable QC workflow to ensure data and process integrity;
4. Cross-validation of InSAR deliverables, including decomposition into vertical and horizontal deformation, with the Groningen GPS (GNSS) network;
5. Deliver a prognostic study of surface deformation at Norg based on InSAR and gas production/injection data;
6. Carry out a quantitative study of shallow compaction over the Groningen area.

References

1. Study and Data Acquisition Plan – Winningsplan 2016, NAM, Jan van Elk and Dirk Doornhof, April 2016
2. Study and Data Acquisition Plan update 2019, NAM, Jan van Elk and Dirk Doornhof, January 2019

NAM

Title	**High resolution InSAR in the Groningen area**	**Date**	November 2019
		Initiator	NAM
Autor(s)	SkyGeo: Yuxiao Qin, Jacqueline Salzer, Hanno Maljaars and Pieter Bas Leezenberg	**Editors**	Jan van Elk Dirk Doornhof
Organisation	SkyGeo	**Organisation**	NAM
Place in the Study and Data Acquisition Plan	Study Theme: Reservoir Compaction Comment: Gas production and the resulting reduction of reservoir pressure cause compaction of the reservoir formation. This is expressed as subsidence at surface, which e.g. requires measures to maintain the ground water level in the area above the Groningen gas field. Subsidence measurements are also used to determine the compaction of the gas reservoir, which drives seismicity in the Groningen area. Monitoring of subsidence is therefore an important activity for NAM. Different techniques are used to monitor subsidence: levelling surveys, GPS-measurements and InSAR satellite observations. Additionally, InSAR offers the opportunity to monitor movement and deformation of infrastructure and larger buildings. This report describes processing of high-resolution radar image data. In the Study and Data Acquisition Plan the objectives of the project were set: 1. Building deformation monitoring; 2. Continuous improvement of InSAR processing and value-adding analysis approaches; 3. Development of visualization tools and establishing an InSAR deliverable QC workflow to ensure data and process integrity; 4. Cross-validation of InSAR deliverables, including decomposition into vertical and horizontal deformation, with the Groningen GPS (GNSS) network; 5. Deliver a prognostic study of surface deformation at Norg based on InSAR and gas production/injection data; 6. Carry out a quantitative study of shallow compaction over the Groningen area.		
Associated research	(1) Development of compaction models based on core measurements. (2) Inversion of subsidence to derive compaction estimates. (3) Seismological modelling.		
Used data	InSAR High-resolution radar image stacks		
Associated organisations	SkyGeo		
Assurance	Internal.		

High resolution InSAR in the Groningen area

2018-2019 Advanced Services

Final Report

Public Report

Date:
Nov 2019

Version:
1.2

Authors:
Yuxiao QIN
Jacqueline Salzer
Hanno Maljaars
Pieter Bas Leezenberg

Account manager:
Pieter Bas Leezenberg

Distribution:
Nederlandse Aardolie Maatschappij B.V.

1. Introduction

In this report, we summarize the results of processing three high-resolution radar image stacks that SkyGeo performed for the NAM. The high-resolution InSAR processing project has been carried out as part of the subsidence data acquisition scope from the 'Study and Data Acquisition Plan Induced Seismicity in Groningen - Winningsplan 2016'. The project involves a semi-continuous InSAR monitoring service, based on ten monthly updates, and six additional services.

The objectives of the high-resolution InSAR project are:

1. Building deformation monitoring;
2. Continuous improvement of InSAR processing and value-adding analysis approaches;
3. Development of visualization tools and establishing an InSAR deliverable QC workflow to ensure data and process integrity;
4. Cross-validation of InSAR deliverables, including decomposition into vertical and horizontal deformation, with the Groningen GPS (GNSS) network;
5. Deliver a prognostic study of surface deformation at Norg based on InSAR and gas production/injection data;
6. Carry out a quantitative study of shallow compaction over the Groningen area.

The main purposes of the project are supporting damage prevention and analysis by high-resolution InSAR building deformation monitoring, and aiding the geomechanical modeling resulting in (predicted) surface deformation as a result of compaction in the hydrocarbon reservoirs. For achieving the aforementioned objectives, SkyGeo aims at providing advanced service components that include, but not limited to, processing, quality control (QC), interpretation, validation and automated reporting for the same period.

This report aims to summarize the outcome of this project in a concise manner. The report is divided into eight sections. Section 2 mentions the SAR dataset used for the project and the area of interest (AoI). Section 3 summarizes the deformation within the Groningen area from the monthly InSAR update reports. Sections 4 to 9 correspond to the six work packages (WP) with the additional services. Specifically:

- Section 4 (WP1): Infrastructure monitoring and building-specific reporting;
- Section 5 (WP2): Quality control (QC) info of updates;
- Section 6 (WP3): Modeling and visualization of the Norg gas storage dynamics;
- Section 7 (WP4): Decomposition and horizontal deformation mapping;
- Section 8 (WP5): Shallow compaction at the Groningen area;
- Section 9 (WP6): Correlation analysis between gas production and surface deformation.
- Section 10 contains the conclusions of this report.

2. Dataset and Area of Interest

The study Area of Interest (AoI) is the Groningen area, where there are known issues of ground subsidence related to gas production activities - and resulting compaction at the reservoir level. Three stacks of TerraSAR-X images in stripmap mode (SM) are used for the AOI. The radar image spatial resolution is 3x3 meters. The details for the three stacks are:

- TSX_DSC_T139 (182 images from Jun 10 2013 to Mar 23 2019);
- TSX_DSC_T63 (201 images from Dec 14 2011 to Mar 29 2019);
- TSX_ASC_T40 (164 images from Jun 25 2013 to Mar 27 2019).

The footprint of the SAR imagery and the AoI is shown in figure 2.1. The naming convention of the three stacks is as follows. “TSX” stands for SAR imagery from the “TerraSAR-X” satellite; “DSC” and “ASC” stand for the descending orbits (images taken from the east, red and blue rectangles) and the ascending orbit (images taken from the west, green rectangle). “T139” stands for “track 139” and means the orbital track from where the images were taken. The track numbers are used to distinguish the two descending tracks.

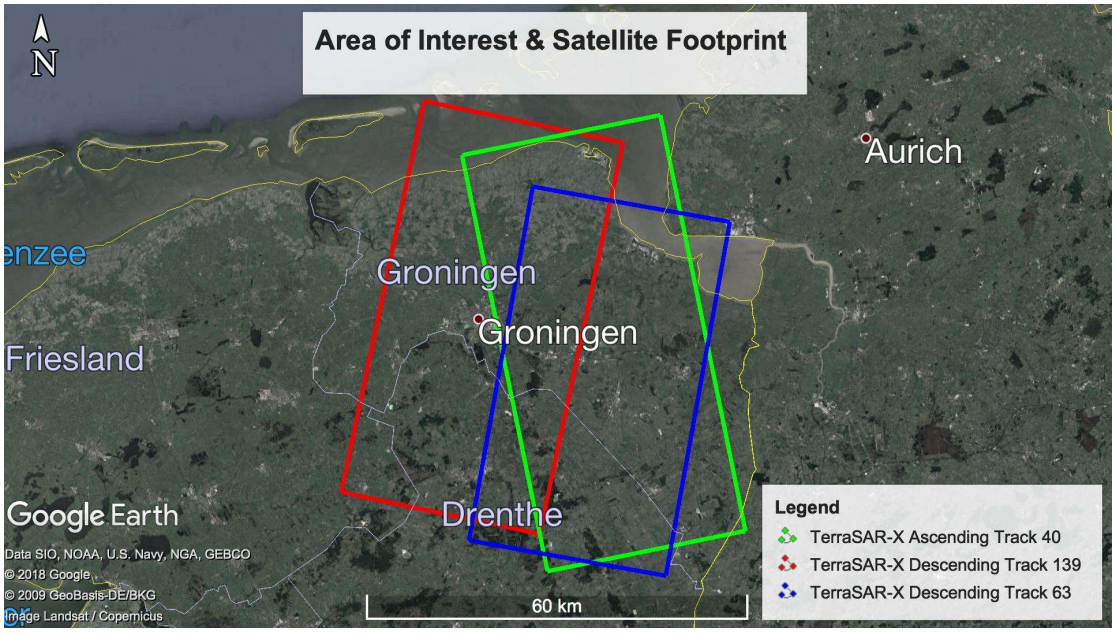

Figure 2.1. The study area of interest and the footprint of the different satellite tracks.

3. Semi-continuous InSAR monitoring service

For the project, SkyGeo delivered 10 monthly updates for the semi-continuous monitoring service. For each of the stacks, the results are categorized into four different groups based on the characteristics of the scatterers: persistent scatterers vs. distributed scatterers; high altitude points vs. low altitude points. The threshold for separating high/low points is 2 meters for the scatterer's relative height to the ground (Actueel Hoogtebestand Nederland, versie 2 (ANH2) data is used for the ground height).

The basic methodology of the semi-continuous InSAR monitoring service, persistent scatterers interferometry (PSI), exploits the persistent targets on the ground that were recorded by synthetic aperture radar (SAR) images. With the continuous and routine acquisition and advanced processing algorithms, SkyGeo is able to retrieve the movement time series in the satellite Line of Sight (LoS) direction on a pixel basis with a measuring precision in the millimeter range. The basic structure of the processing flow is illustrated in Figure 3.1. More background information can be found at the SkyGeo webpage: https://www.skygeo.com/insar-technical-background/.

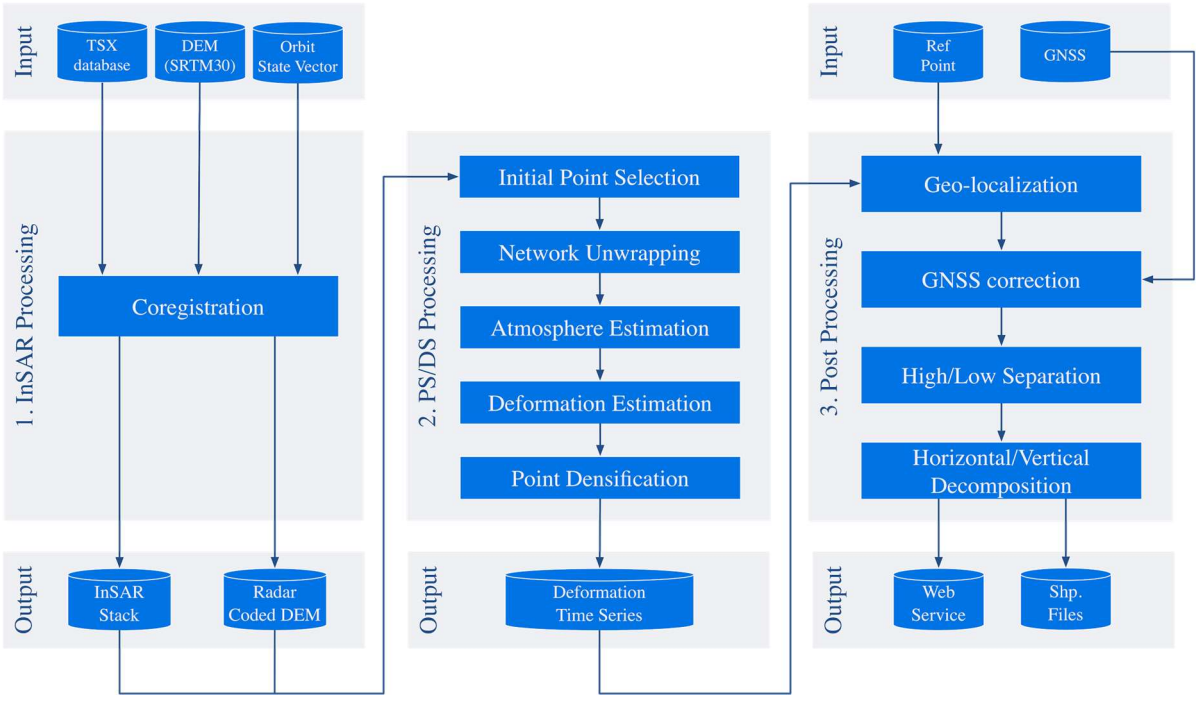

Figure 3.1. A standard workflow diagram of the SkyGeo processing chain for TerraSAR-X. Three main blocks are included: (1) InSAR coregistration; (2) PS/DS processing; (3) Post-processing.

Throughout each update, SkyGeo has made significant contributions towards a finer and higher quality processing, where more advanced algorithms were specially designed for special spots such as the Groningen gas field. The InSAR results are also referenced and cross-validated by GPS data so that a number of refined post-processing steps could be performed with high accuracy, including the

high/low separation, decomposition, shallow compaction and the correlation analysis between InSAR data and the Groningen gas field (see appendix A & B for a more elaborated description on how GPS data are used for referencing/correcting the PS results and for cross-validating the PS results).

The monthly updates have been delivered along with a standardized QC report (see Section 4 for details). The InSAR data also serves as the input to all additional work packages included in this project.

4. WP1: Infrastructure monitoring and building-specific reportings

4.1 Introduction

The output of WP1 is the semi-continuous monitoring service at the individual structure/building level. The point-based InSAR results are aggregated to buildings. The building-specific reports provide a way of evaluating house stability by using deformation measurements collected from individual houses and their surroundings.

4.2 Automated building report

The outlines of the houses used for building analysis are obtained from the open data in the BAG (*Basisregistratie Adressen en Gebouwen*), available in PDOK (www.pdok.nl, *Publieke Dienstverlening Op de Kaart*). Upon clicking on the outline of a building in the SkyGeo Map environment, a report will be generated automatically, summarizing all the available deformation information of the building itself and its surroundings from the available dataset. For each building inside the AoI, a report will be generated upon request, summarizing all the available deformation information of the building itself and its surroundings from the available dataset. An example of such a report page is shown in Figure 4.1.

The characteristics of the TerraSAR-X InSAR results, specifically the high point density, and quality of geolocation and deformation, allow for an analysis of the deformation of individual structures such as buildings. This is generally not possible, or of significantly lower quality, using imagery of lower resolution, like imagery acquired by RadarSat-2 or Sentinel-1. The tool for a per building deformation report demonstrates that the deformation data is readily available through the address of the building. The report can be easily adapted based on the requests of the users.

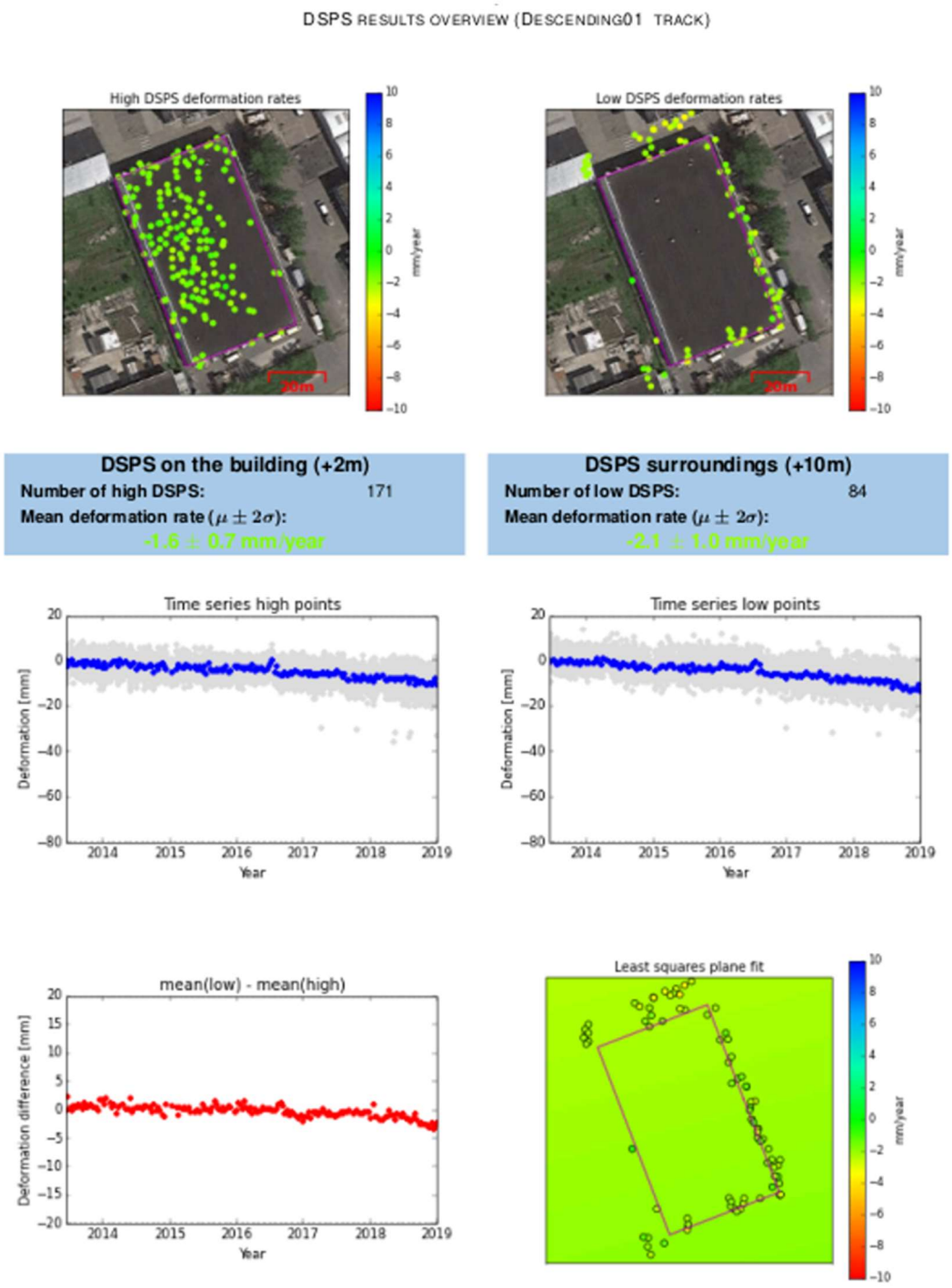

***Figure 4.1**. Sample page of automatically generated report on a single building. Deformation of high and low points is visualized in separate graphs, in the bottom row a more detailed analysis of the differences between high and low is presented. High points are within the 2 meters buffer around the building polygon (taking into account resolution and geolocation error). Low points inside a 10 meters buffer from the building polygon are included. All point scatterers are included in the analysis, Distributed and Persistent Scatterers (DS, PS). The least squares plane fit estimates the deformation rate in the direct vicinity of the building.*

Report description

This report provides an overview of the most relevant statistics for a specific building. The contents on each page are concisely explained here. Each individual page contains the data of a single track. It may occur that a building is not covered by a certain track, and thus no data is present. To retain a constant report structure, these tracks are not omitted from the report, showing empty figures and NaN's instead.

Aerial view plots These plots show the distribution of InSAR points on and near the building. For the selection of high points on the building a buffer of 2 meters is used in order to include points that are on the building but are located just outside the building boundaries. For the selection of low points near the building, a buffer of 10 meters is used. The deformation rate of the points is reflected by their color. Additionally, the outline of the building is drawn.

Statistics The boxes following the aerial view plots contain three relevant figures; the number of points found on or near the building, the mean deformation rate, and twice the standard deviation of the deformation rate. To allow quick visual inspection, the mean deformation rate is also reflected by the text color using the same color scale as used in the aerial view plots.

Time series plots Beneath the statistics boxes, the time series of the absolute deformation associated to the InSAR data points are displayed. The collective data of the selected points is shown as gray dots, and the mean of this data per date as blue dots.

Deformation difference plot This plot shows the difference in mean absolute deformation between low and high points, or the difference between the blue dots in the time series plots. High point deformation is subtracted from low point deformation, such that a downward trend indicates that the terrain has a higher subsidence rate than the building.

Least squares plane fit plot The least squares plot interpolates (and extrapolates) the deformation rate of the low points surrounding the building to provide a continuous estimate of the deformation rate near the building. The interpolation is done by fitting a 2-dimensional linear plane in a least squares way. This plane is defined by:

$$z = c_1 x + c_2 y + c_3,$$

where x and y designate respectively longitude and latitude, and z the resulting deformation rate. The coefficients c_{1-3} are found through solving the following least squares problem:

$$\boldsymbol{c} = \left(\boldsymbol{A}^T \boldsymbol{A}\right)^{-1} \boldsymbol{A}^T \hat{\boldsymbol{z}},$$

where

$$\boldsymbol{c} = \begin{bmatrix} c_1 \\ c_2 \\ c_3 \end{bmatrix}, \quad \boldsymbol{A} = \begin{bmatrix} x_1 & y_1 & 1 \\ \vdots & \vdots & \vdots \\ x_i & y_i & 1 \\ \vdots & \vdots & \vdots \\ x_N & y_N & 1 \end{bmatrix}, \quad \hat{\boldsymbol{z}} = \begin{bmatrix} \hat{z}_1 \\ \vdots \\ \hat{z}_i \\ \vdots \\ \hat{z}_N \end{bmatrix}.$$

Here, N is the amount of data points and $\hat{z}_i$ the deformation rate at location (x_i, y_i). Since 3 coefficients are to be found, at least 3 data points are required to define a consistent system. Less than 3 points will therefore result in an empty plot. **Warning:** This plot should be interpreted carefully, as the way the data is distributed may heavily skew extrapolated data. For example, when the points are approximately located along a line, the gradient of the plane perpendicular to this line is very sensitive to outliers, especially for small amounts of data points.

Figure 4.1. The metadata page of the building report.

5. WP2: Quality control (QC) for the semi-continuous monitoring monthly updates

Within this project, SkyGeo has developed a new automated quality control report that includes the QC of the following items:

- Processing workflow;
- Processing Characteristics and Parameters, i.e., baselines, acquisition information, processing parameters, etc.;
- Atmospheric signal estimation and statistics;
- Point statistics, i.e., density, mean velocity, etc.;
- Validation with GPS data;
- InSAR processing information, i.e., unwrapping errors and arc fixes;
- Decomposition results and validation.

The quality control report is delivered for each monthly update of the semi-continuous monitoring services.

6. WP3: Modeling and visualization of the Norg gas storage dynamics, and the correlation analysis between gas production/storage cycle and surface deformation

This work package was composed of multiple parts:

1. Process the Norg data locally and use GPS data to validate the atmospheric signal estimates in order to obtain optimal estimates of deformation.
2. Create time-lapse visualizations with and without spatial interpretation of deformation signal on a monthly basis.
3. Delineate and create a time-lapse visualization of the deformation boundary (zero signal attributable to reservoir operations).
4. Carry out a historical match analysis to examine and establish correlation between surface deformation and gas production/injection.
5. Explore empirical models that can describe the correlation and use the models to predict deformation and check against InSAR measurements once available.

SkyGeo produced time-lapse visualizations which show the deformation over the Norg area, as well as the storage per well, and its evolution over time, see Figure 6.1. The storage data used were provided by the NAM for this project, the deformation is derived from one track of InSAR data.
Furthermore, we have delivered a detailed report exploring the links between the seasonal gas extraction and the deformation, in which we found that:

- Gas storage volumes and the deformation are strongly correlated, see Figure 6.2.
- A long-term linear trend overlying the seasonal signal of uplift and subsidence.
- The injection through specific wells affects the area affected by the deformation.
- A lag is observed between the time of the maximum/minimum deformation and maximum/minimum of the gas storage, see Figure 6.3. The lag is dependent on the time since operation of the storage as well as the distance to the well.
- A data-driven empirical model (driven by historical storage volumes and deformation) can predict the deformation relatively good for existing well operation scenarios. The model performance can be improved if more data (longer period of observation) is available.

The results of the correlation between gas volume and deformation can be summarized in the form of so-called hysteresis loops, plotting the total storage against the deformation of various points across the reservoir (Fig. 6.3). These pictures show how different points react to the pressure changes induced by the gas. Points close to the wells and centrally located in the reservoir (e.g. the point on the left in Fig 6.3) show tight loops, with the minima of the deformation and gas storage reached at the same time, and the curves returning on a similar path. Points located at larger distances from the main well field, show that the minima in deformation are reached when the gas storage volume

is already increasing. The initially wide loops tighten with time, indicating a decrease in the lag between the gas storage and the deformation.

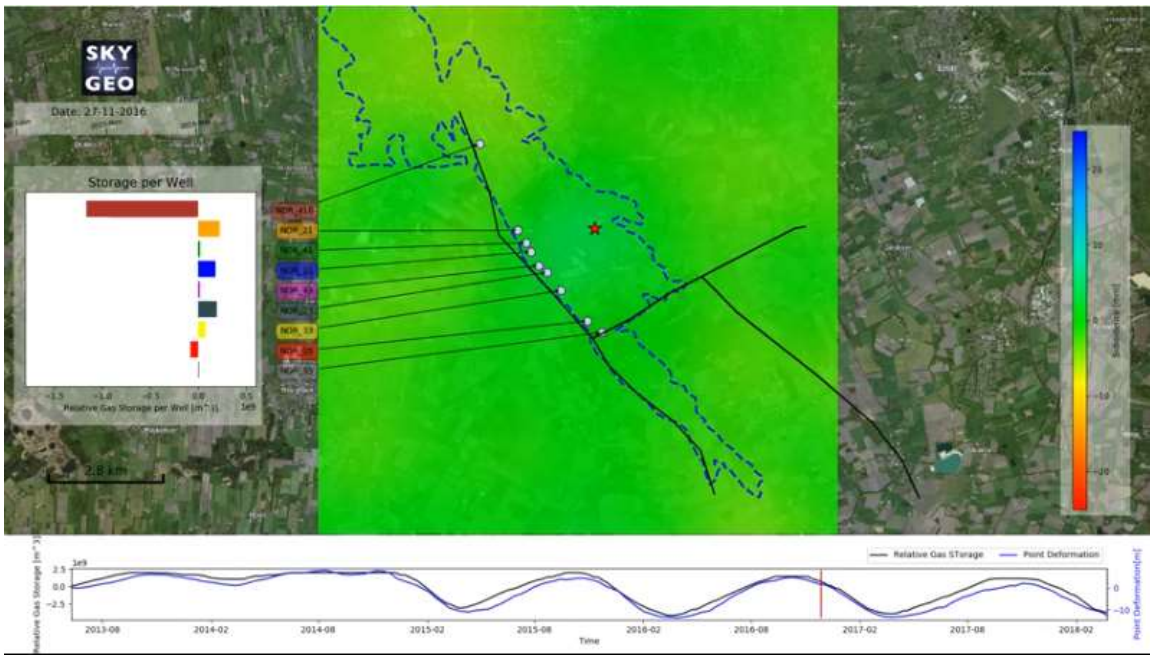

***Figure 6.1**: Screenshot of Norg time-lapse deformation (interpolated from InSAR deformation estimates).*

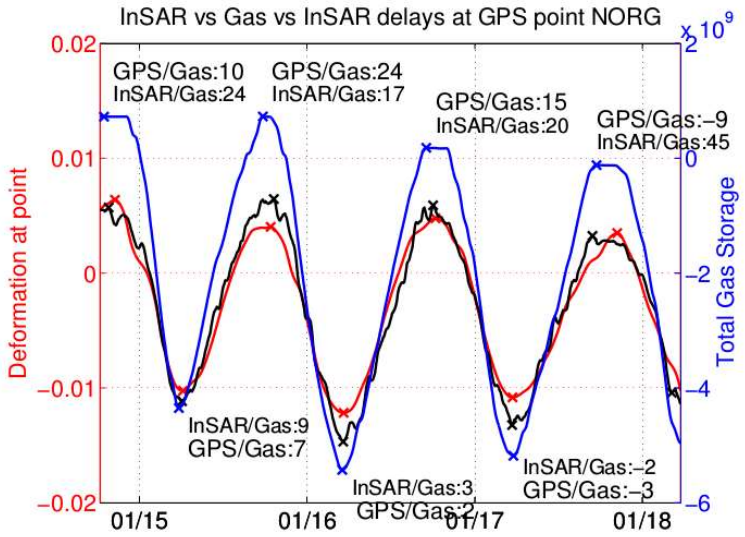

***Figure 6.2**: Deformation of InSAR, GPS and total gas storage at NORG GPS location in metres and cubic metres, respectively. Red curve indicates the InSAR time series, black curve the GPS and blue curve the gas storage. Annotations below and above the curves show the delay in days between the datasets.*

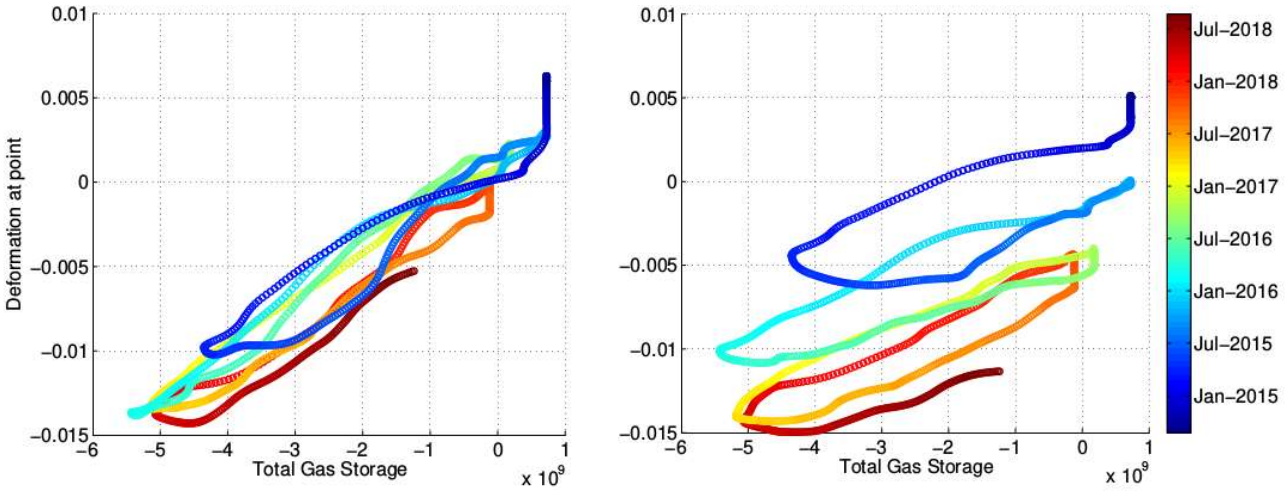

***Figure 6.3**: Two examples of hysteresis loop in the Norg area. Gas storage (m^3) is plotted on x-axis, deformation estimates (m) on y-axis, colored by time. A wide open loop is interpreted as a long lag, a tight loop as no lag. Note the tightening of the loops with time. Besides the seasonal variation, there is a small long-term linear trend as well, which is more prominent in the right figure.*

7. WP4: Decomposition in vertical and East-West deformation

7.1 Introduction

This work package is part of the semi-continuous InSAR monitoring service. Each update includes a horizontal/vertical deformation map using all three stacks. Specifically, the deliverable includes two decomposition maps covering two different areas: one using the asc t40 and dsc t139 datasets, one using the asc t40 and dsc t63 datasets. The decomposition maps include both the horizontal/vertical velocity and the time series. Both velocity and time series are cross-validated with the Groningen GPS network (see Appendix B). In this report, the basic methodology of decomposition will be recapped, followed by results and validation.

7.2 Methodology

InSAR provides a one-dimensional measurement. The measurement is the projection of the ground movement vector to the line of sight (LOS) direction. This is depicted in Figure 7.2. Suppose we have a "true velocity" as shown in Figure 7.2 that is colored in dark red, then from the ascending or descending track measurements alone it is not possible to decompose the vertical and horizontal components without a-priori knowledge or assumptions on the horizontal deformation signal.

However, with one ascending track and one descending track covering the same AoI, the vertical and East-West deformation can be approximated with the following *a-priori* assumption:

> *The contribution of North-South direction movement to the LOS direction, for which the InSAR measurements are largely insensitive due to the imaging geometry, can be neglected.*

If the above assumption holds, the problem becomes a vector decomposition problem in a 2D plane and the solution is unique. The vector decomposition is illustrated in Figure 7.2.

In general, this assumption does hold since the satellite orbits are almost North-South oriented with approximately 10 degrees heading angles. Assuming an incidence angle of 35 degrees, a 10 mm movement in North-South direction would only be 1 mm (*sin(10)*sin(35)*) in the LOS direction.

The basic steps of decomposition are shown in figure 7.1.

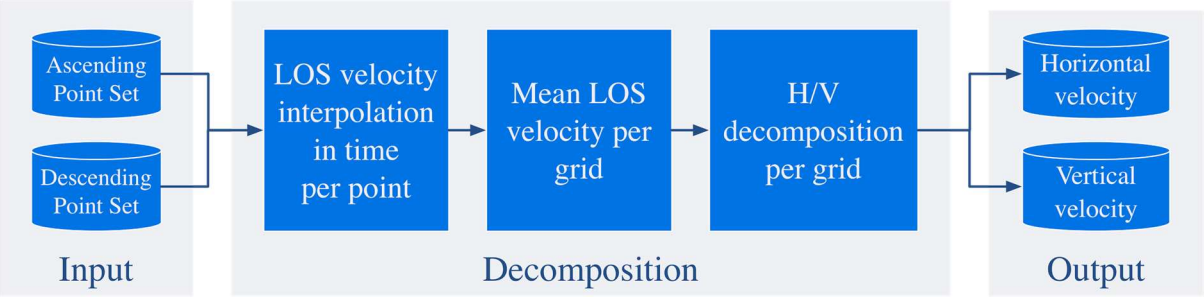

***Figure 7.1**. Workflow for horizontal/vertical decomposition. The decomposition is done using the measurements of all points within grid cells of a predefined size.*

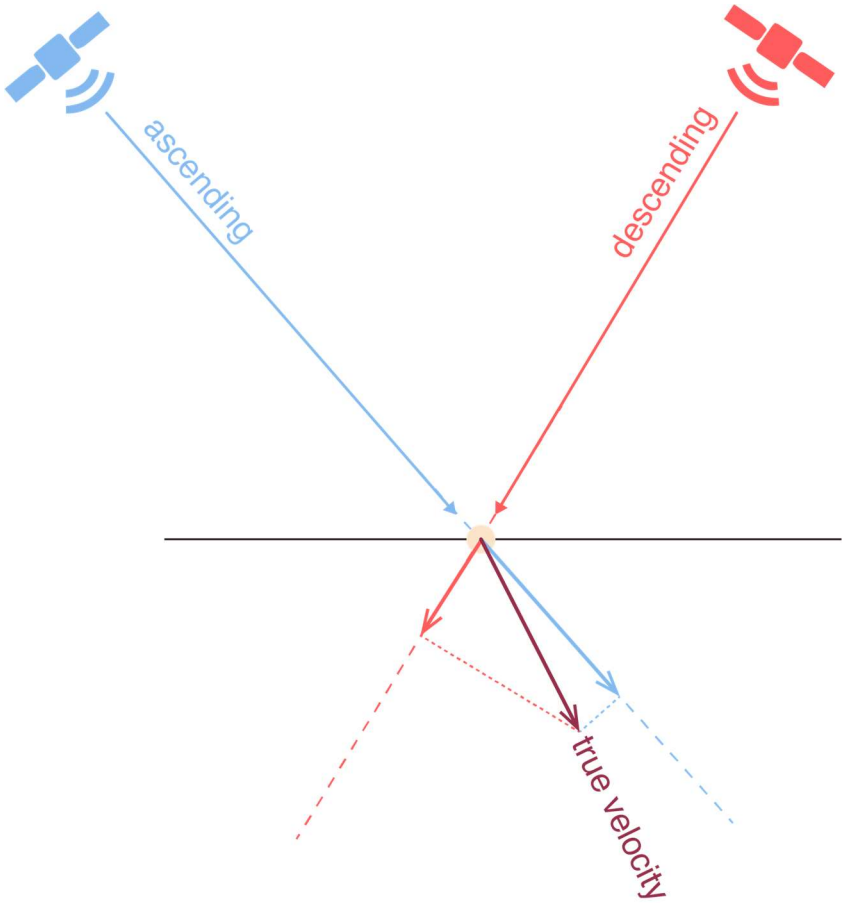

***Figure 7.2**. An illustration of deformation velocity decomposition. Suppose there is a true velocity vector as shown in the figure. The InSAR measurement is the projection to the line of sight direction, shown as the red and blue vectors in the figure. With both descending and ascending deformation estimates available, the true velocity on the vertical-horizontal plane can be calculated by vector addition, and the horizontal/vertical movement can be decomposed from the true velocity vector. Note that this is all based on the assumption that we ignore the North-South direction movement due to the low sensitivity of InSAR to the North-South direction.*

7.3 Results and Validation

7.3.1 Decomposition - linear rates

The resulting linear rates for both combinations of frames are shown in Figure 7.3. All units are in mm/year.

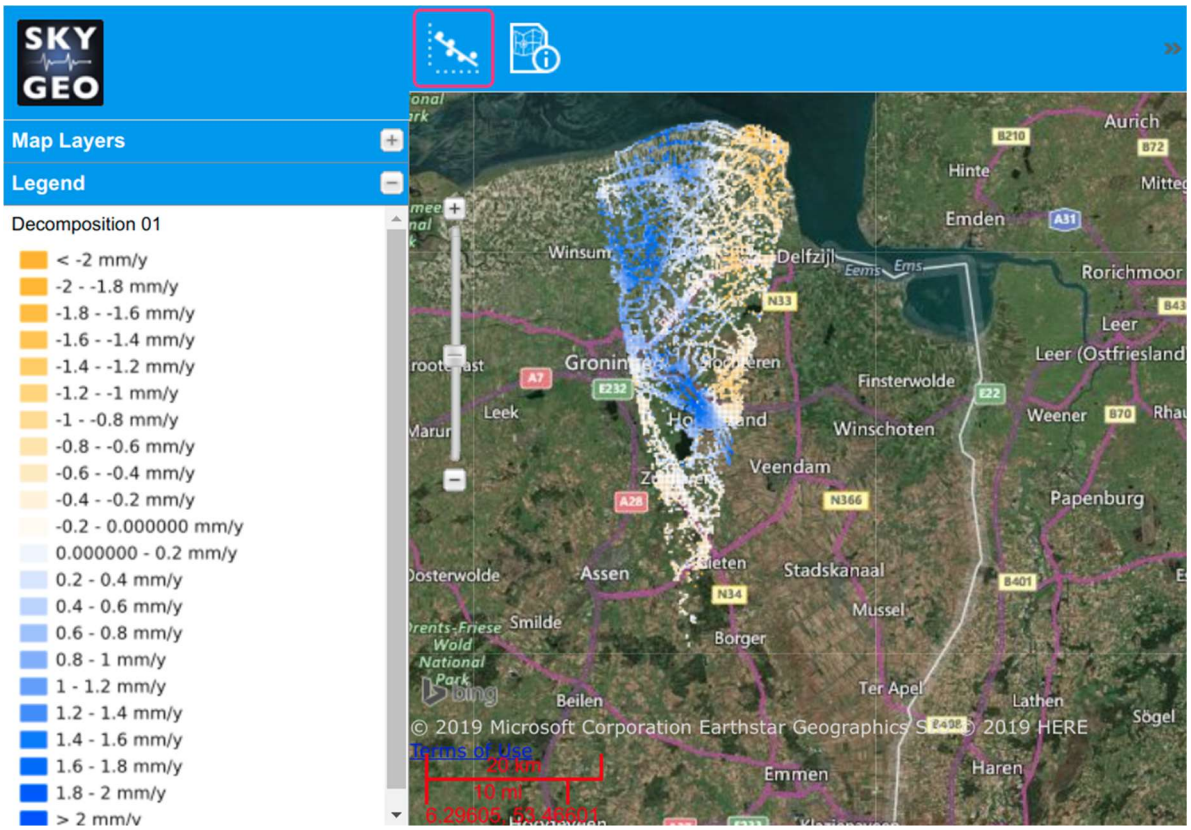

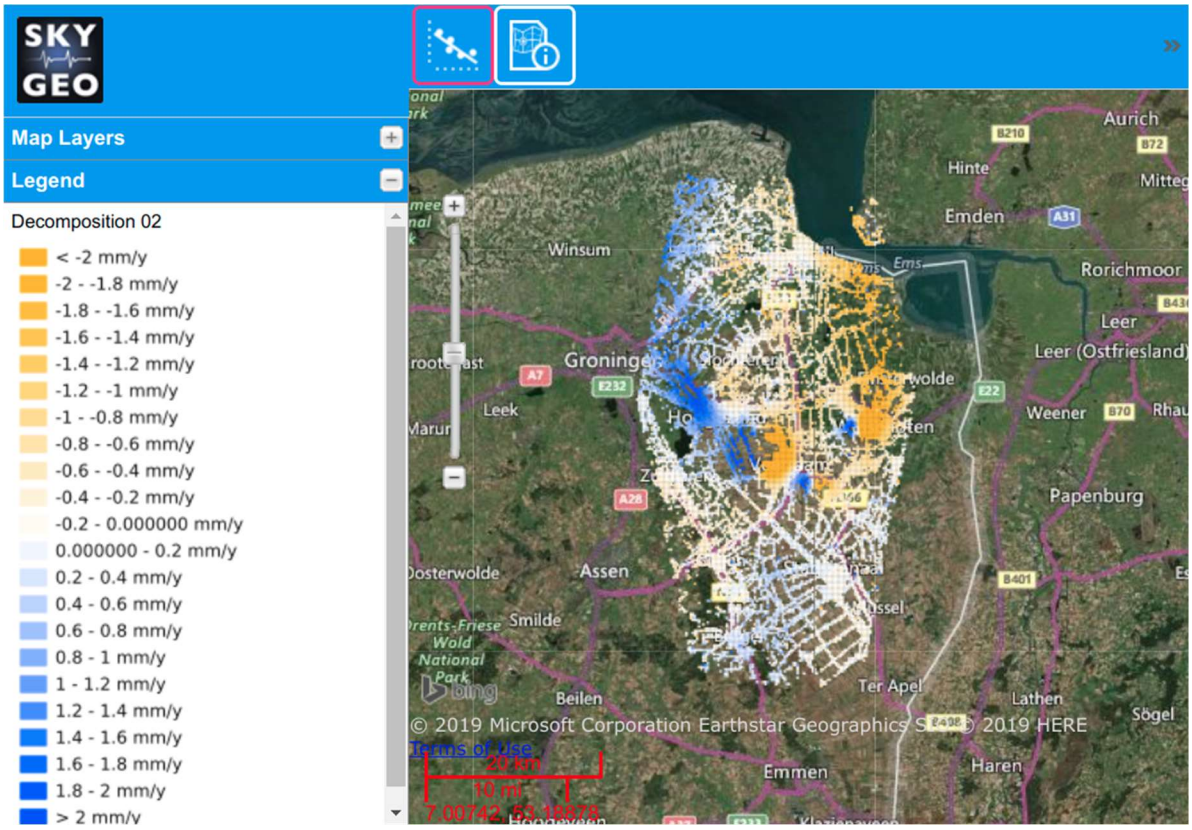

***Figure 7.3**. The linear rates of horizontal movement after the decomposition. Positive (blue) means moving eastward and negative (yellow) means westward. Up: ASC and DSC T139; Down: ASC and DSC63.*

7.3.2 Validation with GPS stations

Appendix B describes the validation between InSAR deformation estimates and GPS data. The overall accuracy of horizontal deformation is reported to be within 1 mm (RMSE) for all GPS stations. One validation result is shown in Figure 7.4 as an example.

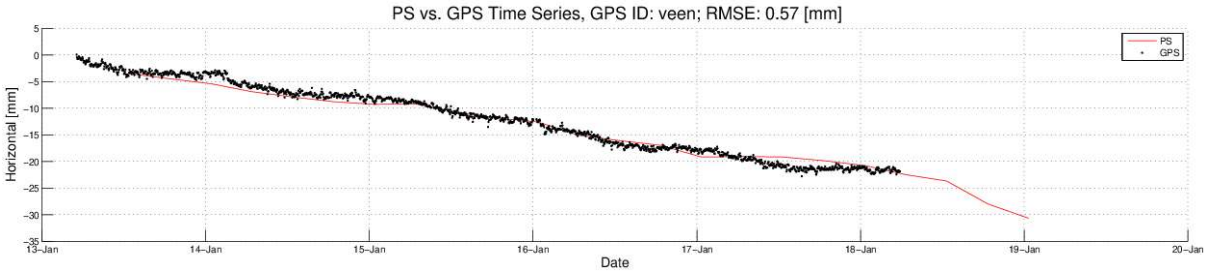

***Figure 7.4**. An example of the validation using a GPS station for the horizontal motion (East-West). The red line shows the decomposition result and the black dots are the GPS measurements.*

7.4 Conclusions and outlook

Based on data presented above and in Appendix B, a few conclusions can be drawn:

- The horizontal deformation is confirmed by the GPS reference stations: there is good agreement between the decomposition results and the GPS-measured velocities for both the vertical and the horizontal (East-West) component.

Outlook:

- The validation and quality assessment of the deformation and decomposition results can be further consolidated with the establishment of a network of radar corner reflectors with an integrated GPS antenna.
- The acquisition of SAR imagery from a combination of a descending and an ascending orbit over the Groningen is the only option for assessing the horizontal component of the deformation with high spatial density.

8. WP5: Shallow compaction in the Groningen area

8.1 Background

This work package studies the shallow compaction inside the AoI from all available stacks. Shallow compaction can occur as a result of the weight that is imposed on the layers, due to a decreasing groundwater level, or due to peat oxidation. The degree of compaction depends on the soil type: clay and peat layers are more affected than sand layers. Furthermore it is dependent on the depth of the layer: deeper layers have already been compacted and an additional pressure increase will have a reduced effect (Ketelaar, V.B.H., Satellite Radar Interferometry: Subsidence Monitoring Techniques, Springer 2009).

SAR satellites can only "see" the combination of shallow and deep subsidence at earth surface level. It requires certain *a-priori* knowledge and assumptions to separate shallow compaction from deep compaction. In this work package, two different methods using different a-priori knowledge are used for calculating the shallow compaction, namely the high-low separation approach and a statistical approach. The methodologies and results are reported in this section.

8.2 Methodology

8.2.1 High-low separation method

One of the logical assumptions is that *houses* are founded on the stable layer that would only be affected by the deep compaction, see Figure 8.1. If this is true, then we should be able to measure deep compaction using scatterers that come from houses. What we would measure from the scatterers elsewhere should be the total compaction (shallow+deep). The difference in terms of subsidence between the two is the shallow compaction.

To separate scatterers that come from houses or ground level, we categorize scatterers into "high points" and "low points" by looking into their 3D positions. For this project, a height of 2 meters with respect to the ground (DEM) elevation is used to separate high and low points. The following steps are performed in order to get the shallow compaction:

1. Grid high and low scatterers into 1000 meters grids;
2. For each grid, calculate the deep compaction from high points, and calculate the total compaction from low points;
3. Shallow compaction is the total compaction minus the deep compaction, hence the average settlement of low points within each grid subtracted by the averaged settlement of the high points.

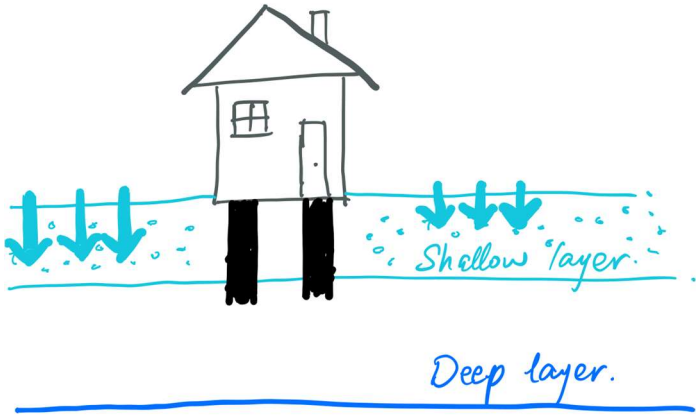

***Figure 8.1**. An illustration of shallow compaction and deep compaction. Houses are well-founded with piles and should only carry the deformation from the deep layer. On the contrary, unfounded structures such as, e.g., roads will be affected by both the deformation of the deep layer as well as of the shallow layer (the high porosity upper layer will compact due to natural processes such as oxidization and degradation).*

8.2.2 The statistical approach

The high-low separation approach is preferred if the heights of the scatterers can be estimated with sufficient precision (for TerraSAR-X ~0.5 m), and the spatial scatterer density is very high. High resolution data such as TerraSAR-x is most suitable for this approach. The statistical approach is proposed as an alternative, and is applicable to any InSAR processing stack in general.

There are a few assumptions for the statistical approach to hold:

1. Within an area, there are scatterers sensitive to total compaction (shallow compaction + deep compaction) and deep compaction (well-founded points). The shallow compaction tends to have a larger velocity than the deep compaction due to natural processes such as oxidation;
2. Within the area, the *majority* of the scatterers come from deep compaction, see Figure 8.2. This is decided by the mechanism behind SAR remote sensing. In SAR imagery, the persistent scatterers (known as 'PS') mostly come from well-founded man-made structures. This indicates that the dominant scatterers are well-founded, deep compacted points. On the other side, the points showing total compaction and come from ground level, only take a small portion.
3. Both the total compaction points and the deep compaction points are normal distributed random variables. This means that, for a small area with either only total compaction points or deep compaction points, the velocity should be normally distributed. Then, for an area with both total compaction and deep compaction, the histogram should be bi-modal with a skewness less than 0.

In reality, because there are far fewer total compaction points than deep compaction points, it is unlikely to observe a clear bi-modal pattern in the histogram. Instead, we see a small "tail" at the left end of the histogram (see Figure 8.3). To determine if there exists shallow compaction (this is equivalent to determine if the "tail" exists), we use the term *skewness*. A histogram with the combination of deep compaction and shallow compaction should have a large negative skewness value (see Figure 8.3).

Figure 8.3 and 8.4 illustrate the idea behind the statistical approach. The approach is as follows:

1. Grid the scatterers using a regular grid size, i.e., 2000 m grid (the grid should be large enough to yield a statistically significant result);
2. For each grid, calculate *the median velocity* and *20% percentile of the scatterers' velocity*. The median velocity represents the deep compaction velocity for this grid, and the 20% percentile velocity indicates the total compaction.
3. The shallow compaction for each grid is the total compaction minus the deep compaction.

***Figure 8.2**. An illustration of the portion of points from deep compaction and from total compaction. The deep compaction comes from buildings and well-founded structures, and the total compaction comes from ground surfaces.*

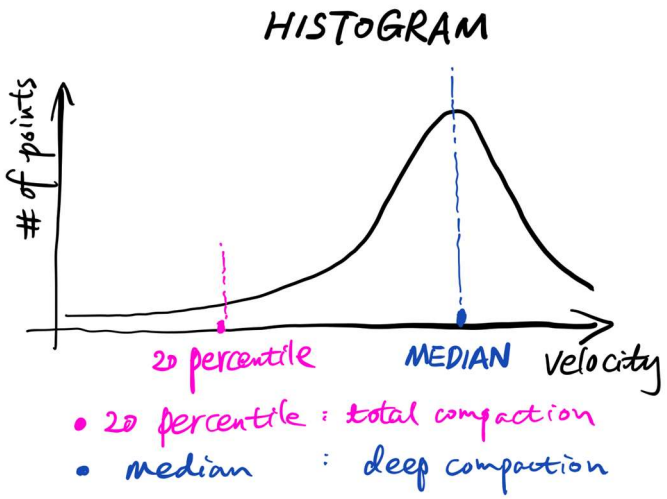

***Figure 8.3**. An illustration of using statistics to estimate the deep compaction and total compaction based on the histogram.*

8.2.3 Considerations of parameters

In the statistical approach, there are three parameters that can be tuned: the size of the grid, the thresholding using skewness, and the percentile to be determined as total compaction velocity.
In this section, we focus on how we selected the statistical approach related parameters: the threshold using skewness and the percentile value.

As discussed in the previous section, if all the scatterers in one grid cell are deep compaction points, then the histogram will look like a normal distribution, symmetric, with skewness value approaching 0. With both deep compaction and shallow compaction points in the grid cell, the histogram will be a little "skewed" to the left, giving a negative skewness value in the histogram. In short, we could use the skewness of the histogram to determine if there is shallow compaction in a given grid. In the bodemdalingskaart project with Sentinel-1 data (www.bodemdalingskaart.nl), an empirical value of -0.7 is used as the threshold. We adopt the same threshold value here.

Regarding the choice of the percentile, ideally, the histogram should be bi-modal with two peaks, one to the right representing the deep compaction and one to the left representing the total compaction. In reality, it is often not possible to see the bi-modal distribution and derive the shallow compaction from it. The workaround is to choose the median as the deep compaction and a percentile value as the shallow compaction. In the bodemdalingskaart project with Sentinel-1 data, an empirical value of 10 percentile is used as the total compaction velocity. However, for the TerraSAR-X satellites, a higher percentile is used (20 %). This percentile is chosen based on comparison with the results of the high-low separation method, which is assumed to be most accurate.

8.3. Shallow compaction assessment and conclusions

Figure 8.4 and figure 8.5 show the shallow compaction calculated from the high-low separation approach and the statistical approach.

We would like to draw a few conclusions based on the results:

- The shallow compaction is present in some areas in our region of interest. However, shallow compaction for the observed persistent scatterers in those areas are mostly limited to about 2 mm/year.
- The correlation between peat layers and shallow compaction is quite distinct once we overlay the shallow compaction layer to the soil type layer. In figure 8.4 and 8.5, places with a pink color (pink color represents peat layers, see https://www.wur.nl/en/show/Grondsoortenkaart.htm for the details of background soil type map) shows stronger shallow compaction with respect to the rest of the places. This coincides with the hypothesis of the mechanism of shallow compaction that was mentioned in Section 8.1.
- The quality of the high-low separation is a clear advantage of TerraSAR-X: it is essential for the assessment of shallow compaction, and will be of great benefit for the comparison with levelling data as levelling benchmarks are commonly found in structures of which the deformation is reflected in the high points.

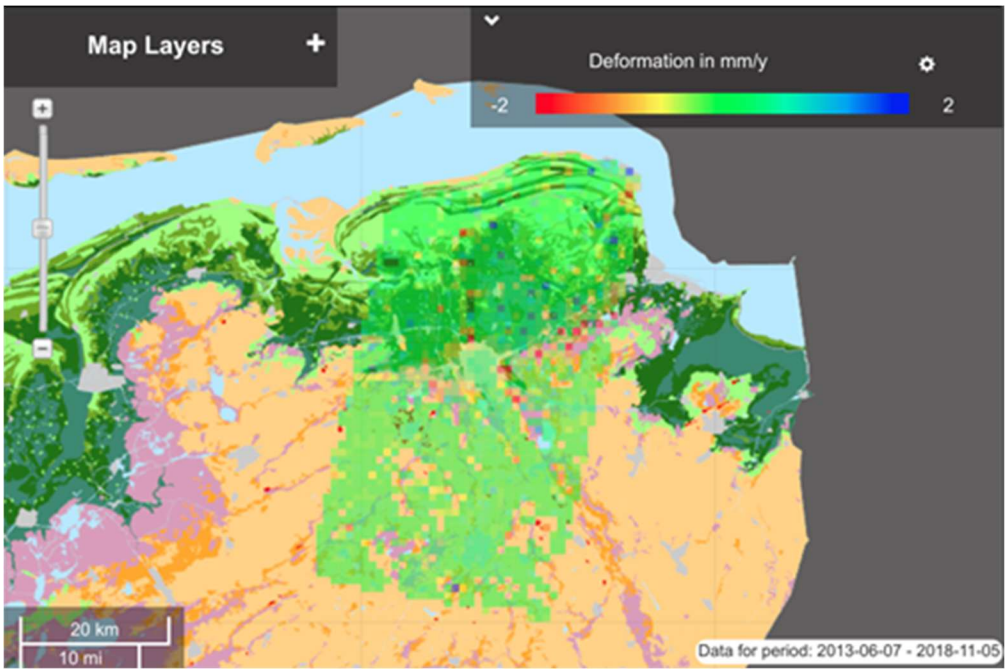

***Figure 8.4**. An example of the shallow compaction velocity estimated by the high-low separation approach for the descending track 139. The grid size is 1000 m. The background layer is the soil type (https://www.wur.nl/en/show/Grondsoortenkaart.htm) where the pink color is the peat layer.*

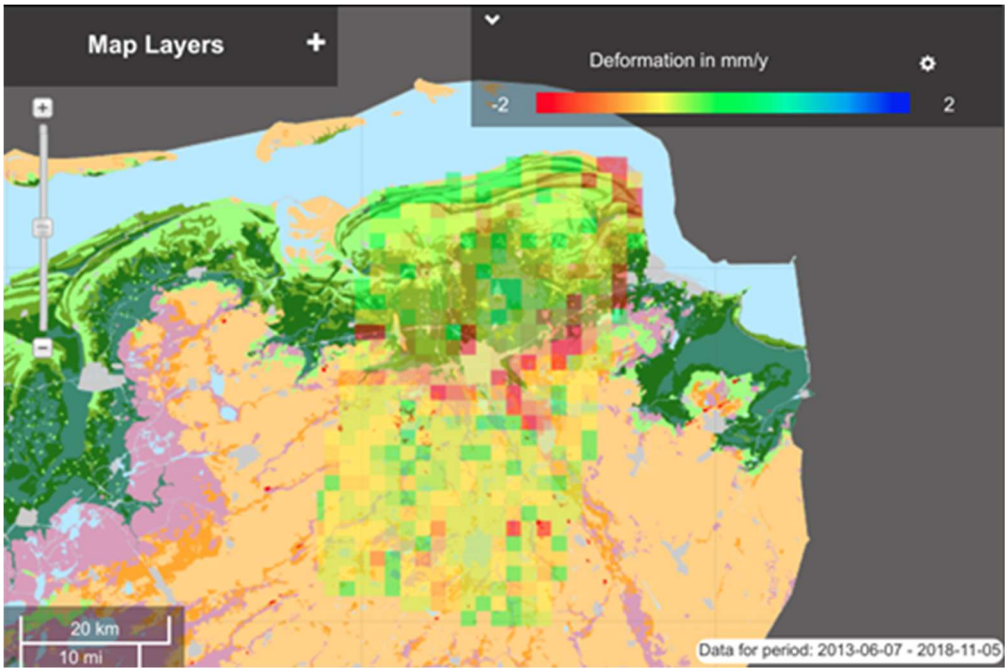

***Figure 8.5**. An example of the shallow compaction velocity estimated by the statistical approach for the descending track 139. The grid size is 2000 m.*

9. WP6: Correlation analysis between gas production and surface deformation

Since around 2013, the total gas extraction from the Groningen area has been decreasing, in particular from the wells in the Loppersum area (Figures 9.1 and 9.2). Subsurface volume change (i.e. gas production) and surface deformation are expected to be correlated. The aim of this work package was analysing whether this can be observed in the Groningen case.

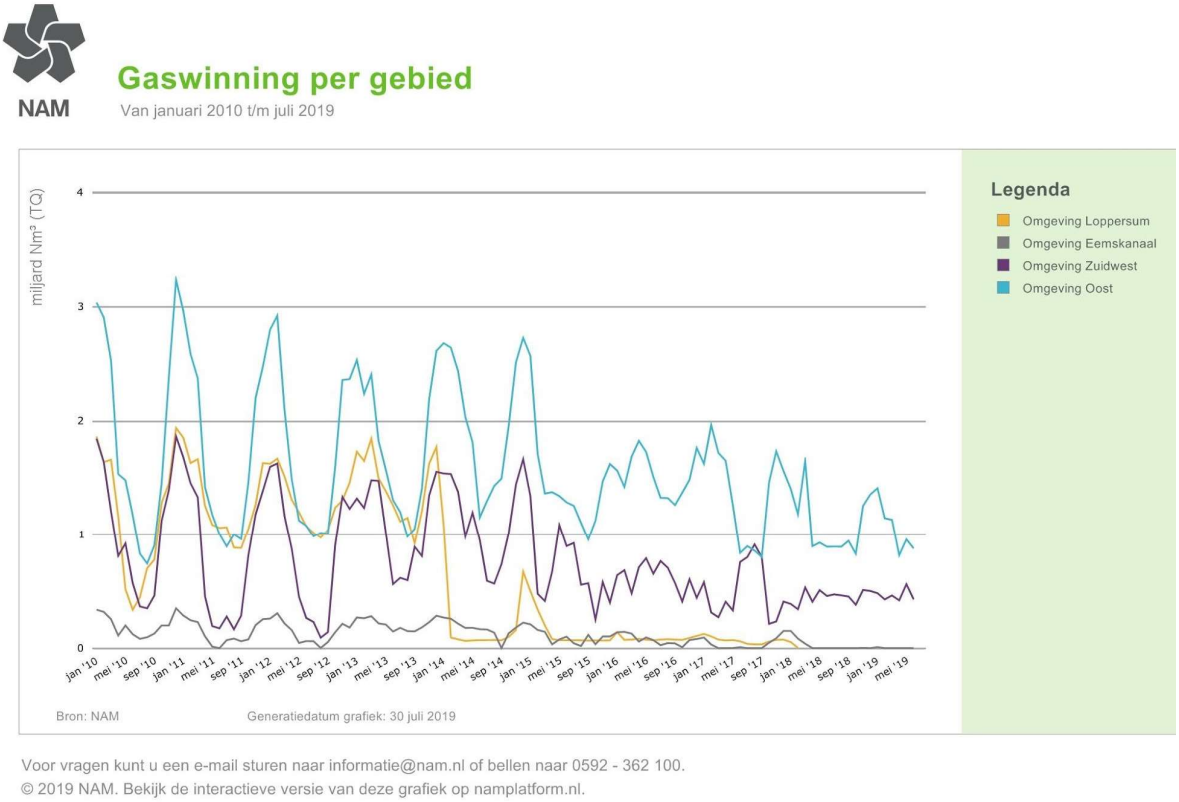

9.1: Identification of deformation related to gas production

In WP5 we have used methods to isolate the shallow compaction. In this work package we use only the deformation derived from the “high” points, since they are more likely to reflect deep deformation originating from the gas reservoir. This applies to both PS and DS “high” points.

SkyGeo has implemented 3 visualization approaches for evaluating deformation along different time periods:

1. Dynamic visualization of deformation along different time periods in a map viewer (see Figure 9.1).
2. Animations to visualize the deformation and the gas production.
3. Figures with cross section of deformation in time.

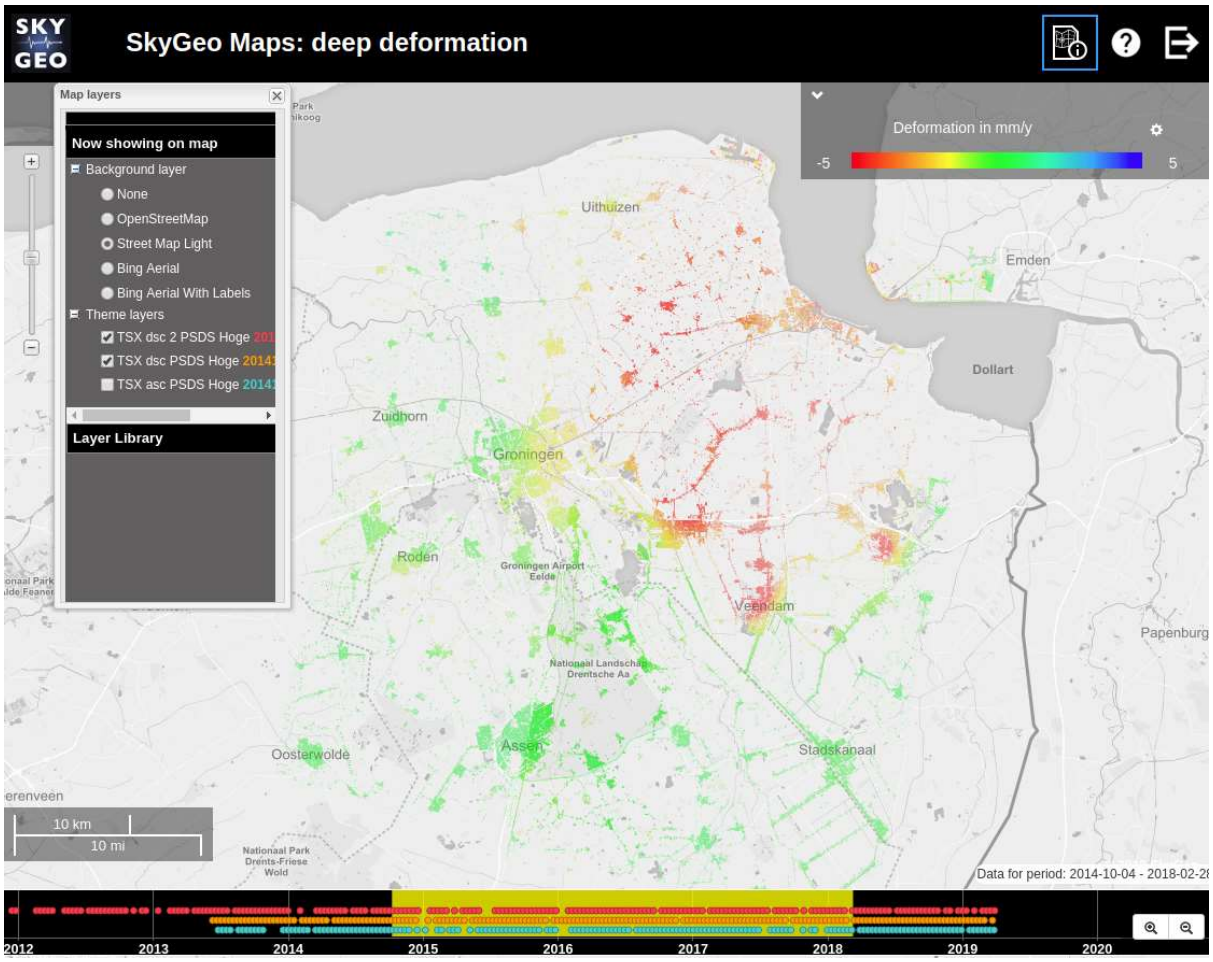

***Figure 9.1**. The SkyGeo map viewer with time-slider capabilities*

The animations have been produced both on the decomposition (vertical and east-west deformation) as well as on the projected line of sight velocities. Animations have been provided at scatterer level, gridded level, and with interpolated, kriged results for deformation.

In each animation, the bar at the bottom shows the production from the 4 different NAM production locations in Groningen (Eemskanaal, Loppesum, Oost, Zuid-West). The color in the map represents the deformation velocity estimated over 9-month period. Note: as opposed to the Norg animations, where we show ***cumulative displacements***, here we show the ***deformation rate***. We choose a 9-month interval since it is a compromise to smooth out short-term atmospheric noise, while preserving seasonal deformation (e.g. from the Norg gas storage). Figure 9.2 shows a screenshot of a Groningen animation.

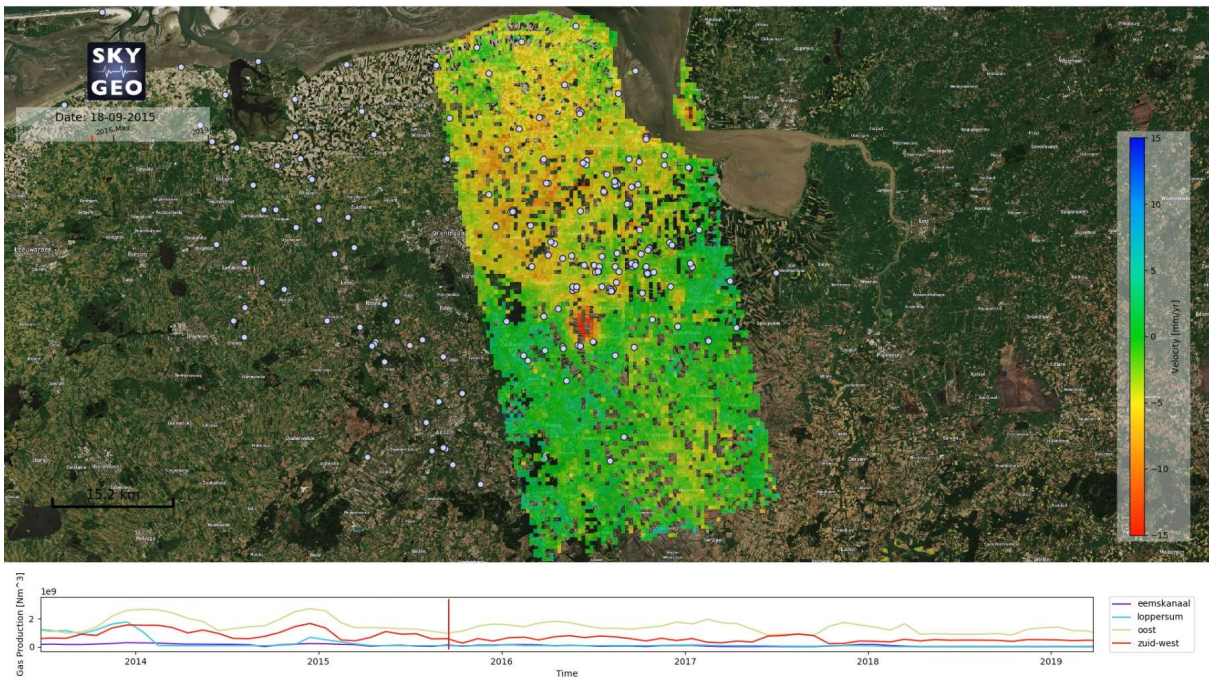

***Figure 9.2**. Screenshot of Groningen animation.*

The series of cross sections across the Groningen area are shown in the figures below (Figs 9.4 - 9.7). The cross sections are plotted based on the decomposition results (Fig 9.3, high points only). The temporal spacing of the lines is constant in time. An increase in the deformation rate therefore leads to an increase in space between successive lines, while a decrease leads to a tightening of the space between the lines.

Analysing the results of the visualizations, we conclude that, up to now, the reduction of the gas production has not had a large effect on the deformation rate.

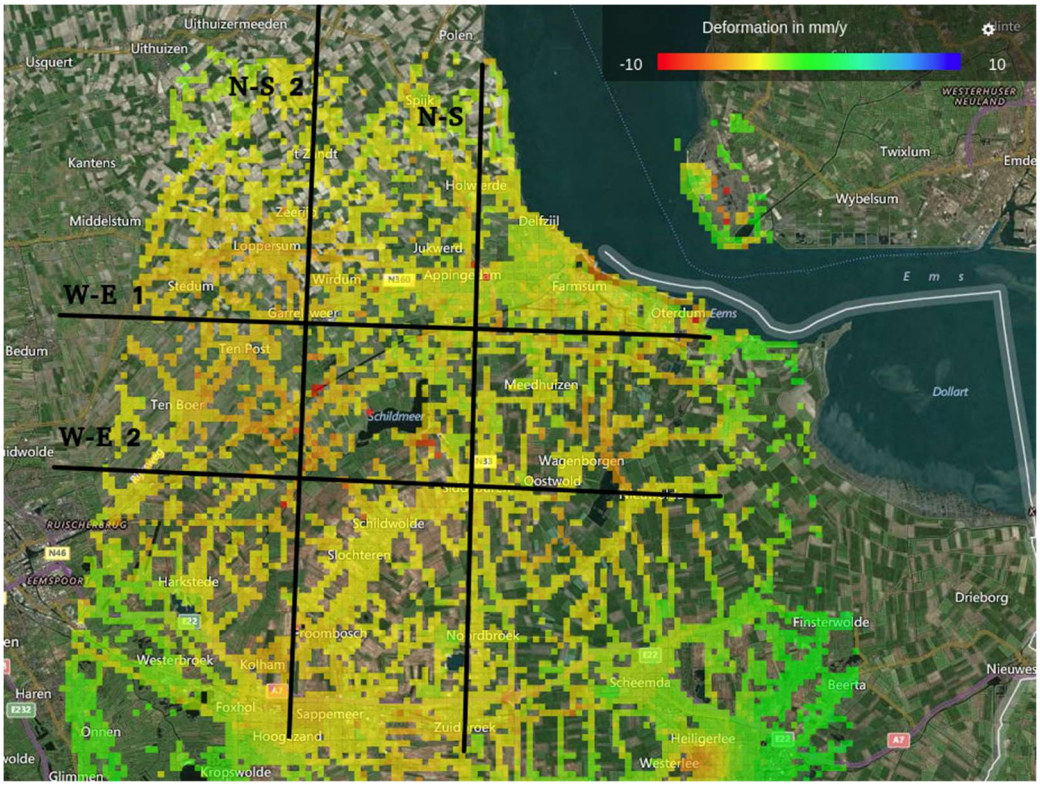

***Figure 9.3**. Locations of cross sections.*

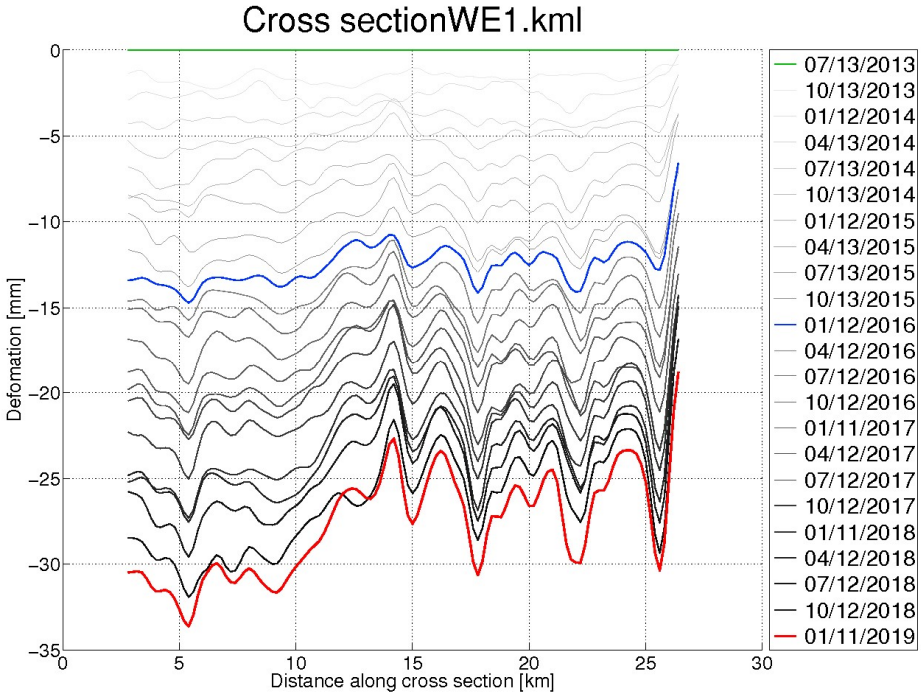

***Figure 9.4**. Cross section W-E 1.*

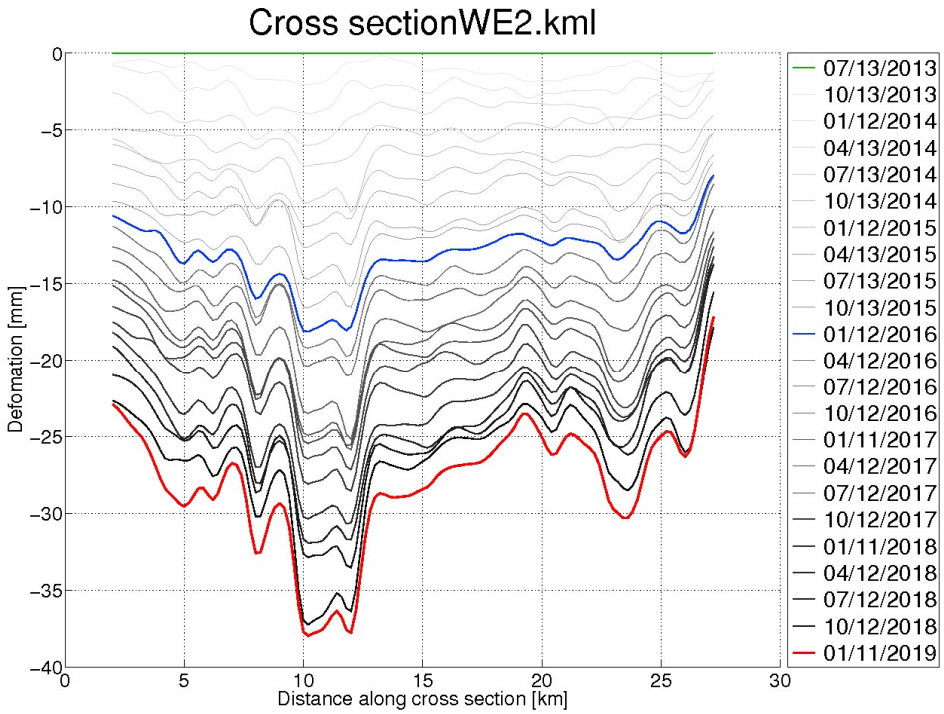

***Figure 9.5**. Cross section W-E 2.*

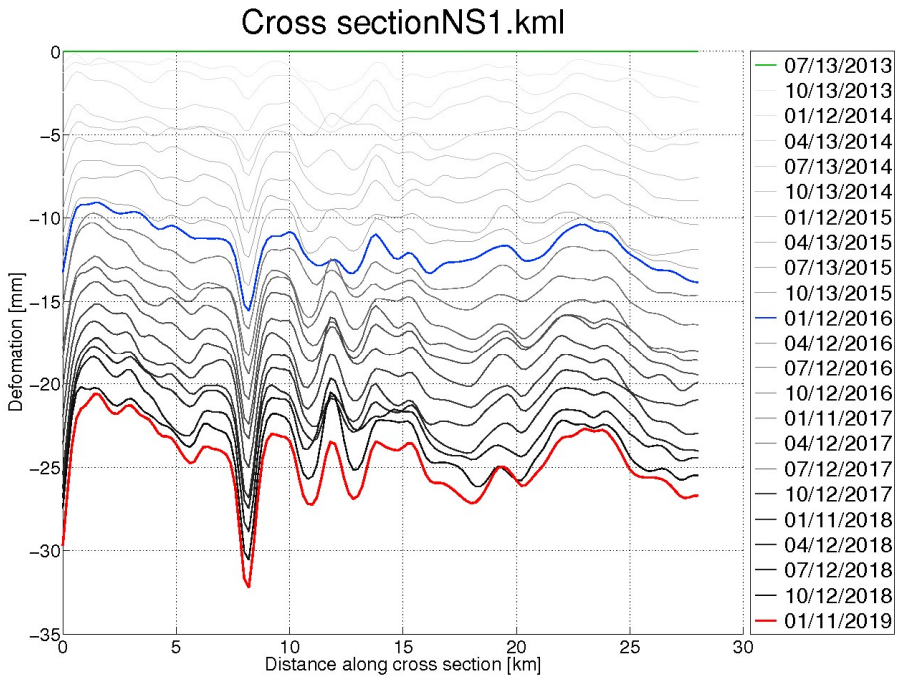

***Figure 9.6**. Cross section N-S 1.*

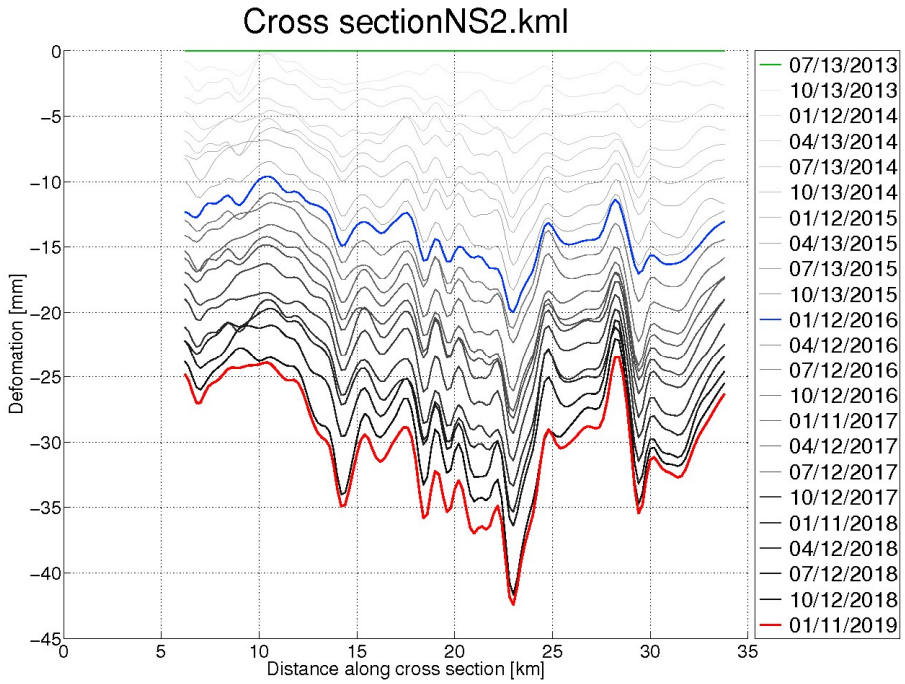

Figure 9.7. *Cross section N-S 2.*

10. Conclusions

SkyGeo monitored subsidence in Groningen by InSAR through the analysis of three partly overlapping high resolution radar image stacks acquired with the TerraSAR-X satellite, two from descending orbits and one from an ascending orbit. The results of the analysis were delivered in a sequence of 10 monthly updates from June 2018 to April 2019. In the last update the total number of images in the 3 stacks approach 550, and the PS-InSAR analysis gives almost 10 million persistent scatterers (PS) and another 6.5 million distributed scatterers (DS) for which the time series were determined. The validation from GPS stations show an overall accuracy of time series (as represented by the RMSE) at mm level and an overall accuracy of the velocity estimate (the difference between GPS measured velocity and PS measured velocity) within 1mm/year (see appendix A).

Deformation data per building has been aggregated for the full area covered by the three frames. Statistics on the deformation represented in all PS on all buildings in the BAG (Basisregistratie Adressen en Gebouwen, an open data set) could be presented. The characteristics of the TerraSAR-X InSAR results, specifically the high point density, and quality of geolocation and deformation, allow for an analysis of the deformation of individual buildings. This is generally not possible or of significantly lower quality with imagery of lower resolution, such as imagery from RadarSat-2 or Sentinel-1.

In this project, the gas storage site Norg has been investigated in more detail. The monitoring of the deformation of the surface in and around Norg showed a sequence of subsidence and uplift with a seasonal difference in height of about 2 cm. The signal turned out to be strongly correlated to the cumulative gas injection and extraction volume. This deformation was validated with the GPS reference station at the NAM site. The conclusion is that near-real time monitoring of the deformation related to the injection-extraction cycle of a reservoir like Norg with a precision close to that of GPS is feasible. Furthermore, the deformation can be approximated well using empirical models based on the deformation and extraction patterns in the previous years, provided that well operations are unchanged.

Horizontal-vertical decomposition was performed in areas where a descending frame overlaps with the ascending frame: in those areas horizontal (East-West) deformation could be approximated with the assumption that the north-south movement could be neglected. Horizontal movements is globally observed in subsidence bowls associated with production, and the Groningen gas field is no exception. The horizontal deformation was confirmed through a validation using GPS reference stations (see appendix B). The acquisition of SAR imagery from a combination of a descending and an ascending orbit is the only option for assessing the horizontal component of the deformation with high spatial density.

Shallow compaction is present in some areas in the area of interest. In order to understand reservoir compaction and dilation we want to account for this factor numerically. Maximum shallow

compaction rates for InSAR measurement points reach about 2 mm/year in those areas, and is very much correlated with the presence of peat layer at those locations. The overall shallow compaction rates at other places are rather limited to within the 2mm/yr range.

The deformation monitoring project over Groningen described in this report clearly demonstrates the capability of InSAR with very high resolution imagery of a satellite like TerraSAR-X.

Appendix A. Use of GPS for referencing and validation

A.1 How is GPS used for referencing and validation

During the process, two types of external measurements are used for referencing and validation purposes. The first type is GPS measurements and the second type is the stable points (strong scatterers in areas that are not affected by surface deformation).

In the referencing stage, a selected number of GPS measurements and all stable points are used as the reference. The linear rates are calculated and converted to line-of-sight. A plane least-squares estimation is applied to estimate the offset between GPS referencing points and the InSAR measurements. For the least-squares estimation, the InSAR-measured-points within 50m buffer of the referencing point are selected for calculating the mean velocity and for the least-squares adjustment. Finally, all linear deformation rates are corrected according to the least square estimation. The same linear deformation rate corrections are applied to the time series of deformation estimates.

In the validation stage, more GPS measurements are added for validating the velocity and time series of PS measurements.

A.2 Velocity Validation

The velocity validation between GPS and PS is reported below. For each GPS point, the InSAR-measured-points within 50m buffer of the GPS point are selected, their mean velocity is calculated. Each GPS point is represented with a four-letter name. Stable points are strong scatterers taken from the known stable areas (not affected by surface deformation). Stable points are designated as "stable" followed by two digits numbers. The GPS stations and stable points used for both the correction and validation are highlighted in bold blue.

A.2.1 DSC_T139

Table: TSX_DSC_T139: The Validation between GPS and InSAR Measurement. Unit: mm/yr

Reference point		InSAR measurements within 50 meters buffer			
Name	Velocity	Mean velocity	Velocity std. deviation	No. of points	Velocity difference
eems	**-3.7**	**-3.8**	**1.38**	**499**	**-0.1**
froo	-4.9	-4.5	0.67	450	0.4

over	-3.8	-3.7	0.45	572	0.1
sted	-4.5	-4.7	0.23	199	-0.2
tenp	-5.3	-4.6	0.39	514	0.7
usqu	-0.8	-0.8	0.35	214	0
zand	-4.2	-4.1	0.34	495	0.1
zeer	-5	-5.1	1.14	125	-0.1
stable01	0	-0.1	0.58	141	-0.1
stable03	0	0.1	0.48	197	0.1
stable05	0	-0.1	0.52	84	-0.1
stable08	0	-0.1	1.23	150	-0.1
stable09	0	-0.1	0.72	348	-0.1
stable14	0	0.1	0.49	455	0.1
stable18	0	0.4	0.42	153	0.4
stable23	0	-0.2	0.83	306	-0.2

A.2.2 DSC_T63

Table: TSX_DSC_T63: The Validation between GPS and InSAR Measurement. Unit: mm/yr

Reference point		InSAR measurements within 50 meters buffer			
Name	Velocity	Mean velocity	Velocity std. deviation	No. of points	Velocity difference
0647	-2	-1.9	1.3	429	0.1
dzyl	-3.5	-4	0.61	647	-0.5
eems	-3	-2.8	0.82	722	0.2
froo	-4.7	-3.8	0.7	670	0.9
over	-3	-3.1	0.44	856	-0.1
sted	-3.8	-3.8	0.3	245	0
tenp	-4.8	-4.1	0.4	788	0.7
tjuc	-3.3	-3.3	0.54	467	0

veen	-7.3	-6	0.38	462	1.3
zand	**-3.4**	**-3.3**	**0.36**	**866**	**0.1**
zdvn	-3.6	-2.9	0.36	842	0.7
zeer	-4.4	-4.3	0.86	84	0.1
stable01	**0**	**-0.2**	**0.6**	**117**	**-0.2**
stable04	**0**	**0.4**	**0.39**	**425**	**0.4**
stable05	**0**	**-0.2**	**0.49**	**94**	**-0.2**
stable07	**0**	**0.2**	**0.48**	**152**	**0.2**
stable08	**0**	**-0.1**	**0.98**	**223**	**-0.1**
stable11	**0**	**-0.3**	**0.78**	**498**	**-0.3**
stable15	**0**	**0.1**	**0.62**	**353**	**0.1**
stable19	**0**	**-0.1**	**0.43**	**612**	**-0.1**

A.2.3 ASC_T40

Table: TSX_ASC_T40: The Validation between GPS and InSAR Measurement. Unit: mm/yr

Reference point		InSAR measurements within 50 meters buffer			
Name	Velocity	Mean velocity	Velocity std. deviation	No. of points	Velocity difference
0647	0.2	-0.6	0.84	321	-0.8
dzyl	-2.9	-3.6	0.63	553	-0.7
eems	**-4.3**	**-4**	**0.86**	**585**	**0.3**
froo	-3.7	-3.6	0.72	594	0.1
over	**-3.3**	**-3.3**	**0.58**	**686**	**0**
sted	-4.3	-4.9	0.24	194	-0.6
tenp	-4.7	-4.5	0.5	665	0.2
tjuc	-2.5	-2.5	0.73	377	0
usqu	**-1.2**	**-1.7**	**0.4**	**177**	**-0.5**

veen	-2.4	-1.6	0.26	343	0.8
zand	**-4**	**-3.6**	**0.4**	**505**	**0.4**
zdvn	-3.2	-2.9	0.42	664	0.3
zeer	-4.4	-4.8	1.13	173	-0.4
stable01	**0**	**0.2**	**1.32**	**142**	**0.2**
stable04	**0**	**0.1**	**0.53**	**472**	**0.1**
stable05	**0**	**-0.1**	**0.28**	**25**	**-0.1**
stable07	**0**	**-0.1**	**0.34**	**67**	**-0.1**
stable11	**0**	**0**	**0.65**	**351**	**0**
stable15	**0**	**0**	**0.73**	**342**	**0**
stable16	**0**	**0.1**	**0.26**	**7**	**0.1**
stable17	**0**	**0**	**0.47**	**381**	**0**
stable19	**0**	**-0.1**	**0.39**	**456**	**-0.1**
stable21	**0**	**-0.3**	**0**	**1**	**-0.3**
stable22	**0**	**0.2**	**0.48**	**461**	**0.2**

A.3 Time Series Plot: GPS vs PS

In this section, we compare the GPS measurements (converted to satellite LoS direction) with the InSAR measurements. In sequence, the following steps are performed for the comparison:

1. For each GPS point, we select PS points within the 50m buffer and take their average time series;
2. We plot the GPS time series vs. averaged PS points time series. It should be noted that both GPS and InSAR are relative measurements in time so that one could select an arbitrary starting value. In this report, we set the first value in PS time series to 0, and adjust the GPS time series (by adding or subtracting a constant value) so that the sum of the difference between GPS and PS time series is minimized. Note that this “alignment” is only for plotting purposes. It changes neither the estimated velocity of GPS and PS, nor the root mean square error between GPS and PS.
3. For the statistical comparison between the two measurements, we perform a correlation analysis and calculate the root mean square error (RMSE). The RMSE is an indication of the InSAR measurement accuracy. Note that the RMSE here is independent of the constant value adjustment for GPS in the previous step. The complete steps for the correlation analysis can be found in "*Yuxiao Qin, Monitoring Ground Subsidence in Hong Kong via Spaceborne Radar: Experiments and Validation, Remote Sensing, 2015; DOI:10.3390/rs70810715*".

A.3.1 DSC_T139

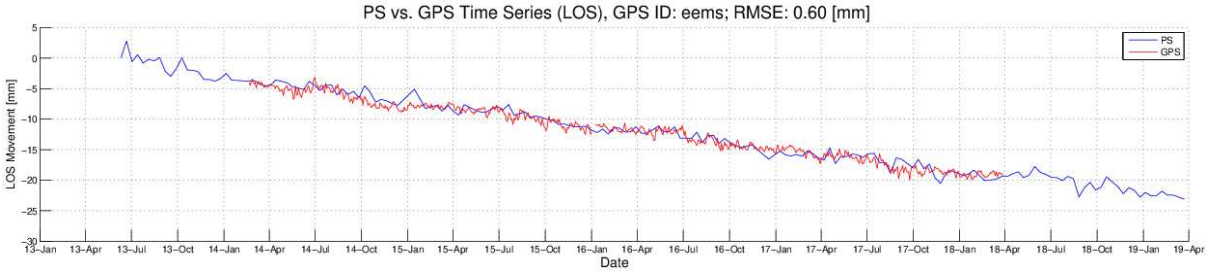
PS vs. GPS Time Series (LOS), GPS ID: eems; RMSE: 0.60 [mm]
LOS Movement [mm]
Date
PS
GPS

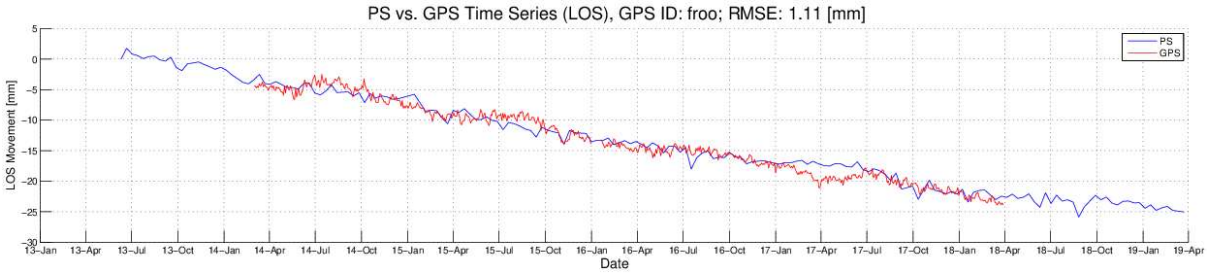
PS vs. GPS Time Series (LOS), GPS ID: froo; RMSE: 1.11 [mm]
LOS Movement [mm]
Date
PS
GPS

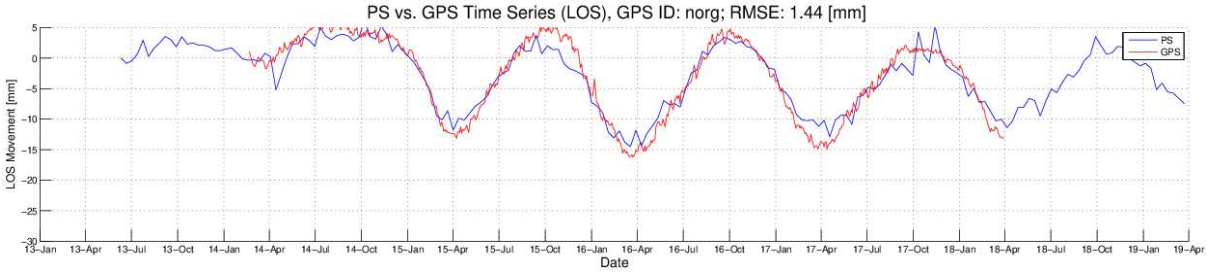
PS vs. GPS Time Series (LOS), GPS ID: norg; RMSE: 1.44 [mm]
LOS Movement [mm]
Date
PS
GPS

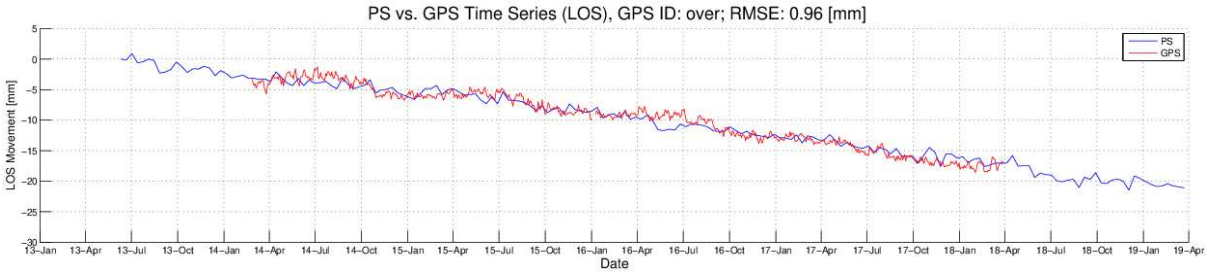
PS vs. GPS Time Series (LOS), GPS ID: over; RMSE: 0.96 [mm]
LOS Movement [mm]
Date
PS
GPS

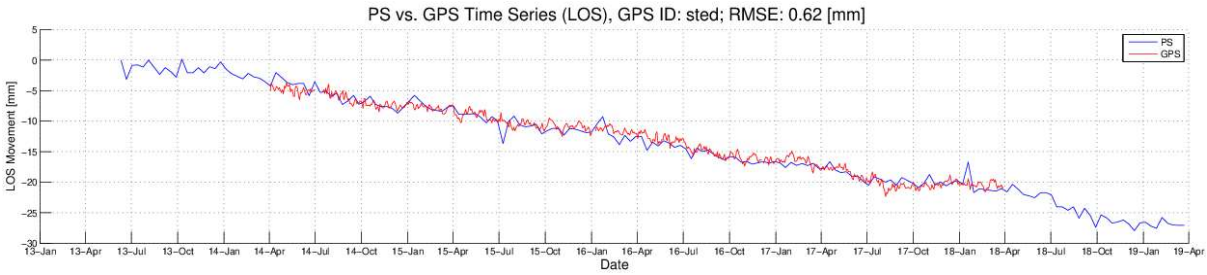
PS vs. GPS Time Series (LOS), GPS ID: sted; RMSE: 0.62 [mm]
LOS Movement [mm]
Date
PS
GPS

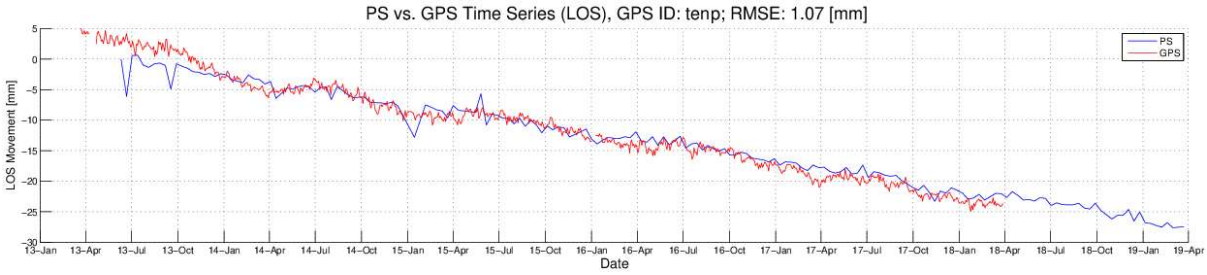
PS vs. GPS Time Series (LOS), GPS ID: tenp; RMSE: 1.07 [mm]
LOS Movement [mm]
Date
PS
GPS

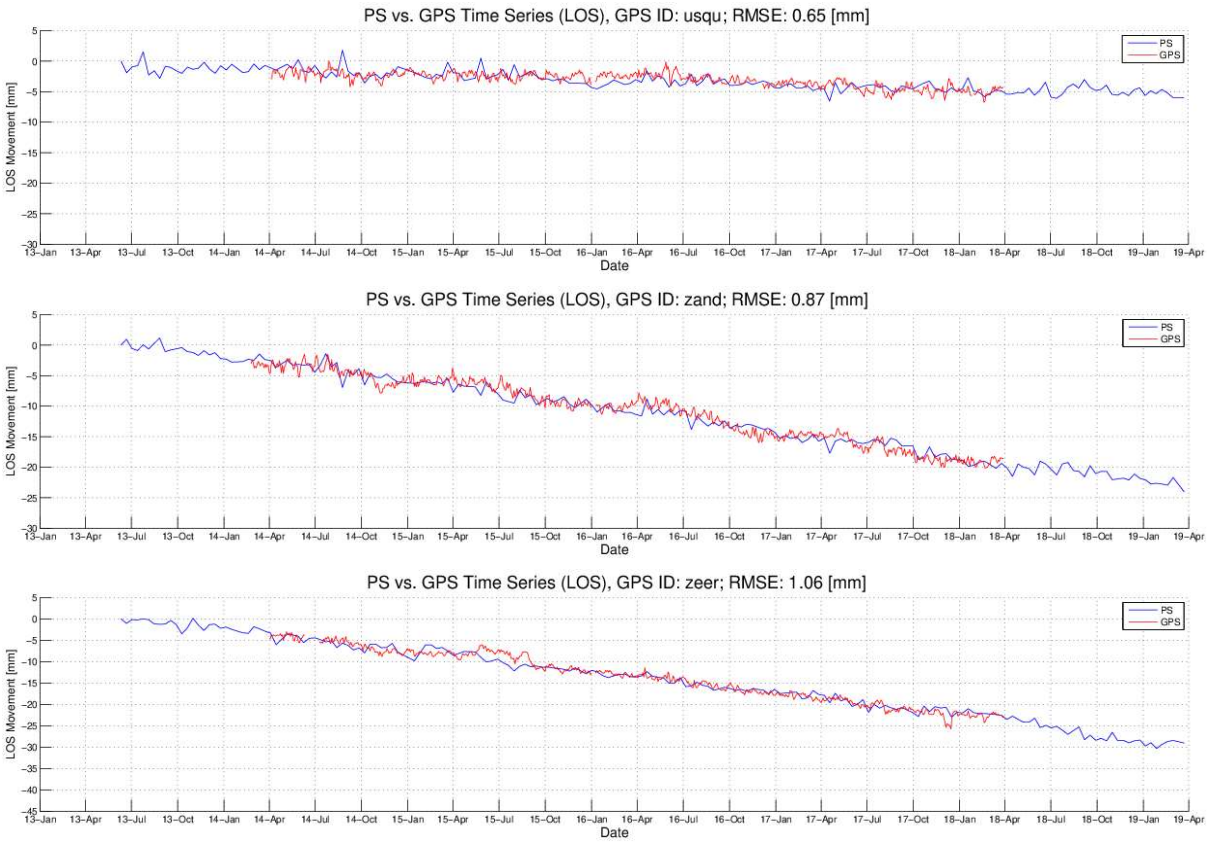
PS vs. GPS Time Series (LOS), GPS ID: usqu; RMSE: 0.65 [mm]
PS vs. GPS Time Series (LOS), GPS ID: zand; RMSE: 0.87 [mm]
PS vs. GPS Time Series (LOS), GPS ID: zeer; RMSE: 1.06 [mm]
LOS Movement [mm]
Date
PS
GPS

A.3.2 DSC_T63

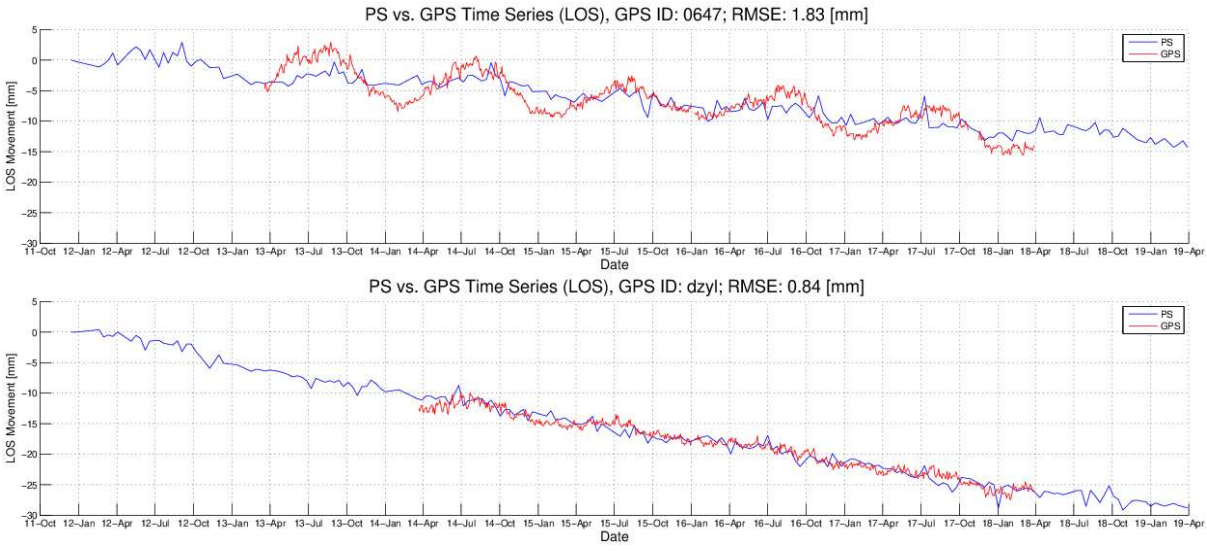
PS vs. GPS Time Series (LOS), GPS ID: 0647; RMSE: 1.83 [mm]
PS vs. GPS Time Series (LOS), GPS ID: dzyl; RMSE: 0.84 [mm]
LOS Movement [mm]
Date
PS
GPS

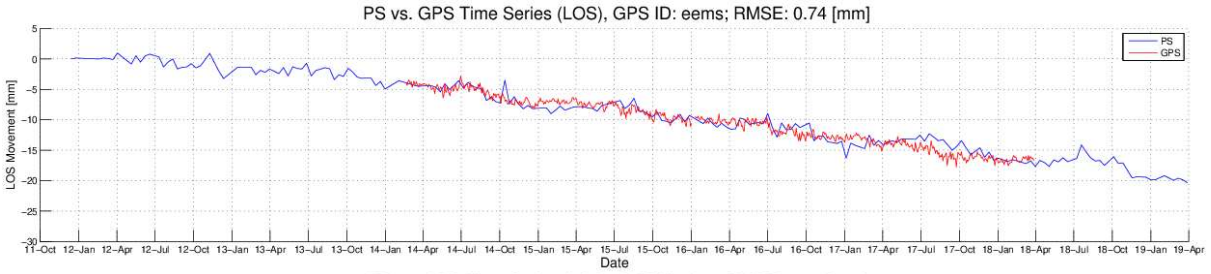
PS vs. GPS Time Series (LOS), GPS ID: eems; RMSE: 0.74 [mm]
LOS Movement [mm]
Date
PS
GPS

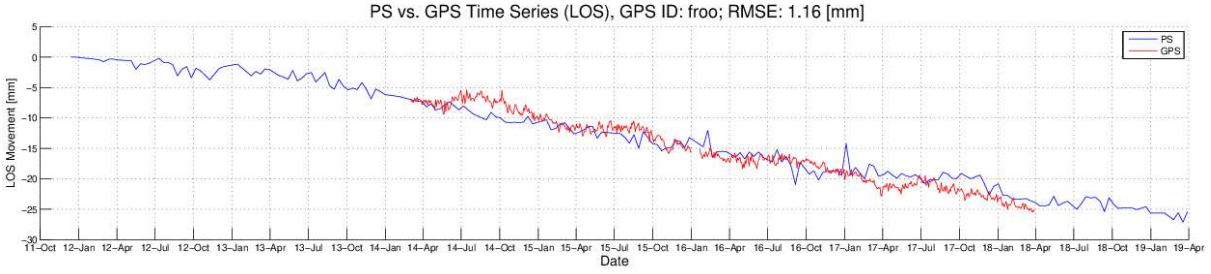
PS vs. GPS Time Series (LOS), GPS ID: froo; RMSE: 1.16 [mm]
LOS Movement [mm]
Date
PS
GPS

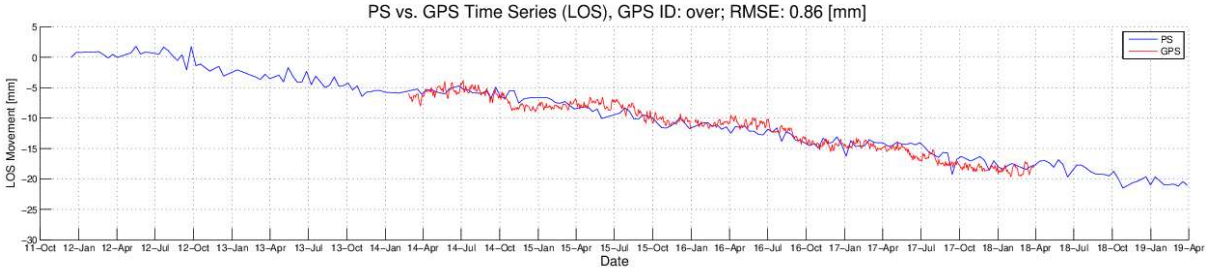
PS vs. GPS Time Series (LOS), GPS ID: over; RMSE: 0.86 [mm]
LOS Movement [mm]
Date
PS
GPS

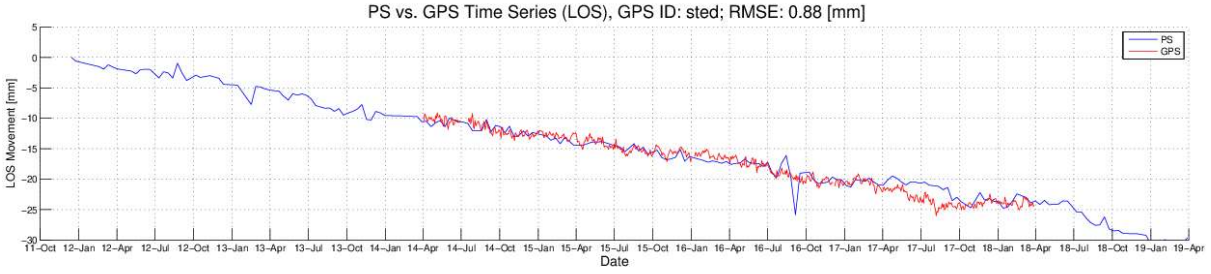
PS vs. GPS Time Series (LOS), GPS ID: sted; RMSE: 0.88 [mm]
LOS Movement [mm]
Date
PS
GPS

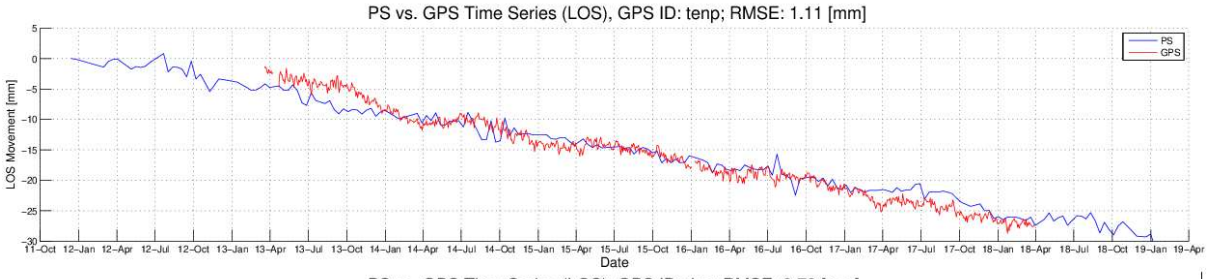
PS vs. GPS Time Series (LOS), GPS ID: tenp; RMSE: 1.11 [mm]
LOS Movement [mm]
Date
PS
GPS

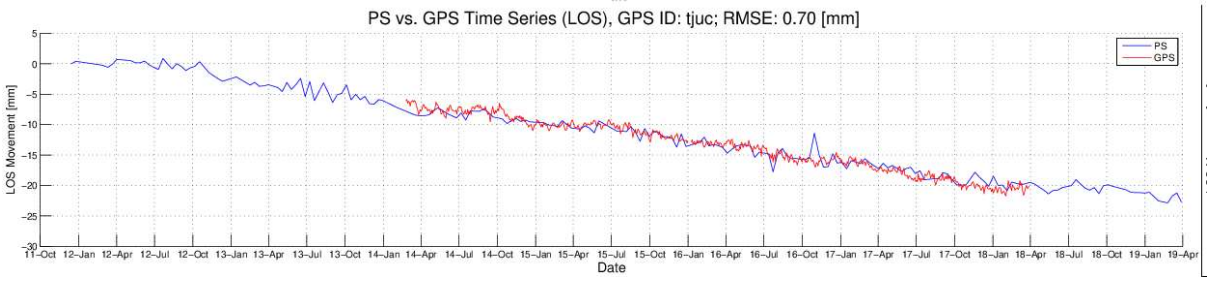
PS vs. GPS Time Series (LOS), GPS ID: tjuc; RMSE: 0.70 [mm]
LOS Movement [mm]
Date
PS
GPS

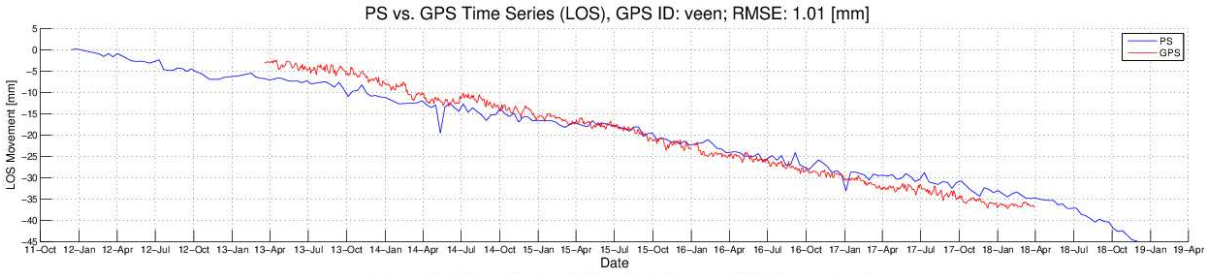
PS vs. GPS Time Series (LOS), GPS ID: veen; RMSE: 1.01 [mm]
LOS Movement [mm]
Date
PS
GPS

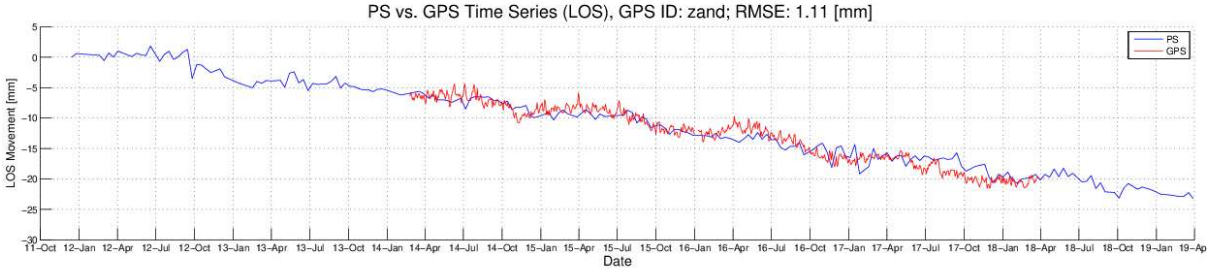
PS vs. GPS Time Series (LOS), GPS ID: zand; RMSE: 1.11 [mm]
LOS Movement [mm]
Date
PS
GPS

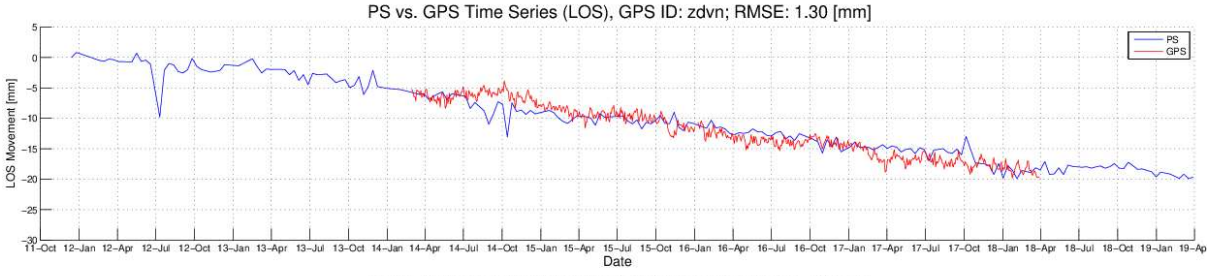
PS vs. GPS Time Series (LOS), GPS ID: zdvn; RMSE: 1.30 [mm]
LOS Movement [mm]
Date
PS
GPS

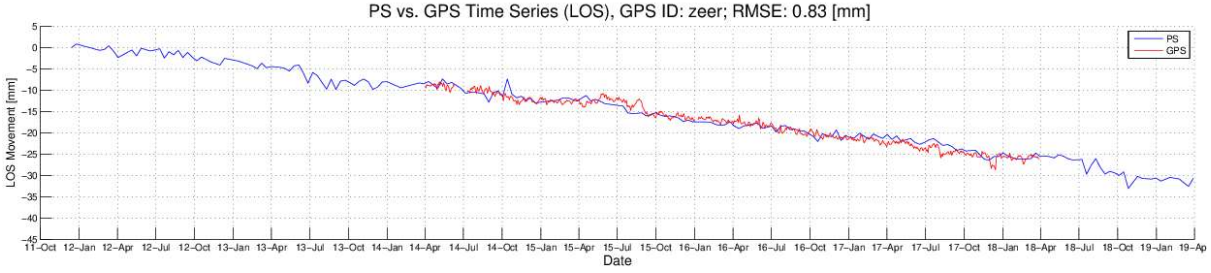
PS vs. GPS Time Series (LOS), GPS ID: zeer; RMSE: 0.83 [mm]
LOS Movement [mm]
Date
PS
GPS

A.3.3 ASC_T40

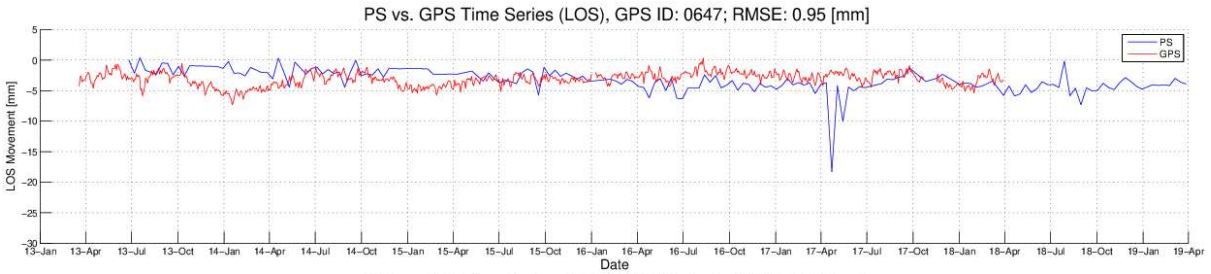
PS vs. GPS Time Series (LOS), GPS ID: 0647; RMSE: 0.95 [mm]
LOS Movement [mm]
Date
PS
GPS

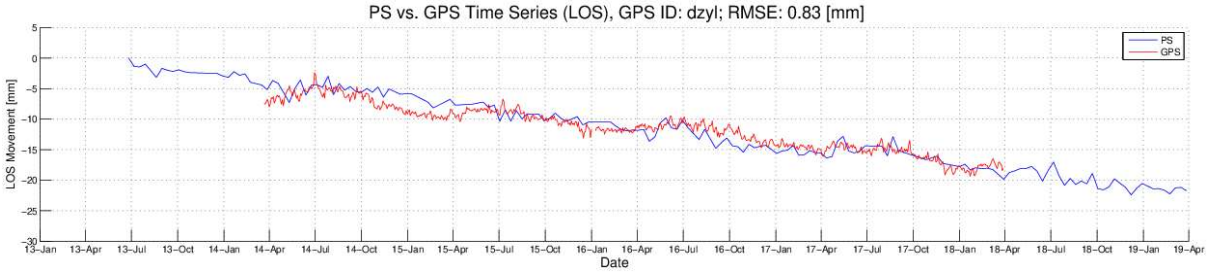
PS vs. GPS Time Series (LOS), GPS ID: dzyl; RMSE: 0.83 [mm]
LOS Movement [mm]
Date
PS
GPS

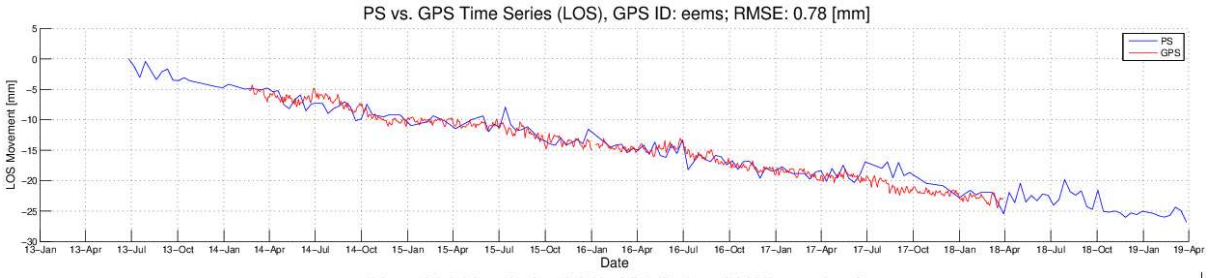
PS vs. GPS Time Series (LOS), GPS ID: eems; RMSE: 0.78 [mm]
LOS Movement [mm]
Date
PS
GPS

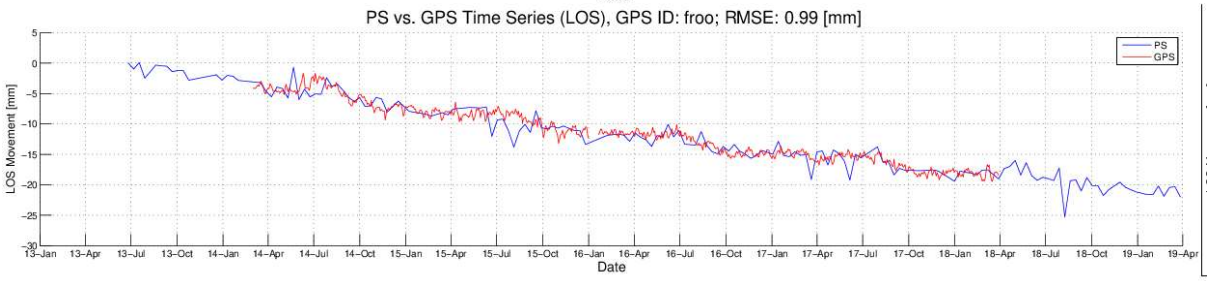
PS vs. GPS Time Series (LOS), GPS ID: froo; RMSE: 0.99 [mm]
LOS Movement [mm]
Date
PS
GPS

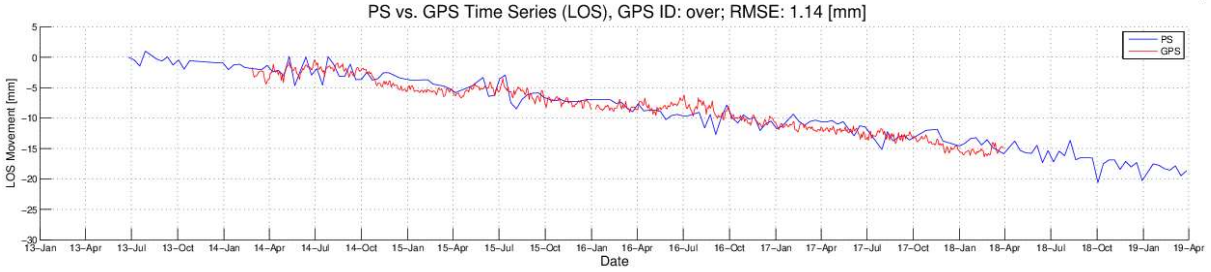
PS vs. GPS Time Series (LOS), GPS ID: over; RMSE: 1.14 [mm]
LOS Movement [mm]
Date
PS
GPS

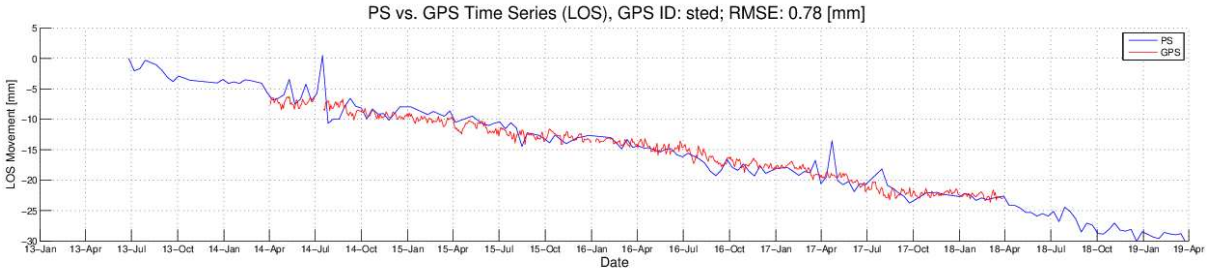
PS vs. GPS Time Series (LOS), GPS ID: sted; RMSE: 0.78 [mm]
LOS Movement [mm]
Date
PS
GPS

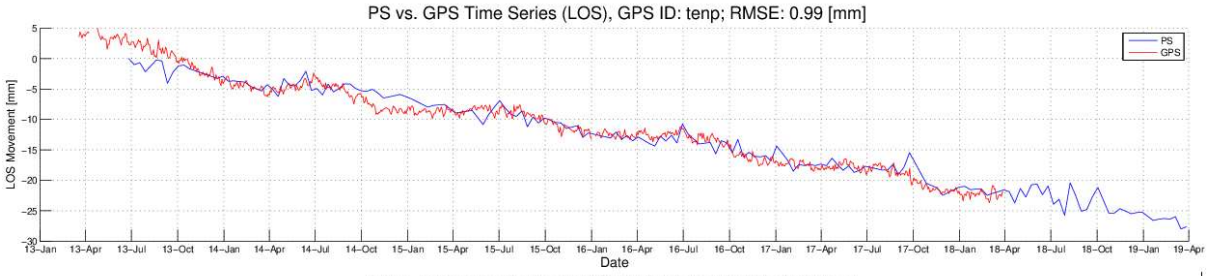
PS vs. GPS Time Series (LOS), GPS ID: tenp; RMSE: 0.99 [mm]
LOS Movement [mm]
Date
PS
GPS

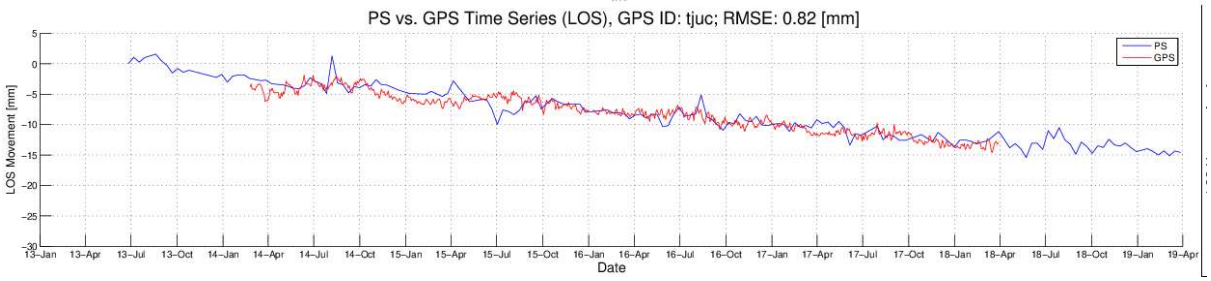
PS vs. GPS Time Series (LOS), GPS ID: tjuc; RMSE: 0.82 [mm]
LOS Movement [mm]
Date
PS
GPS

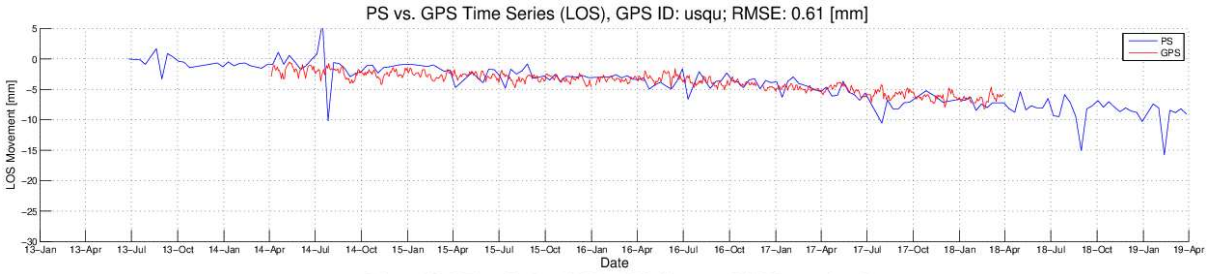
PS vs. GPS Time Series (LOS), GPS ID: usqu; RMSE: 0.61 [mm]
LOS Movement [mm]
Date
PS
GPS

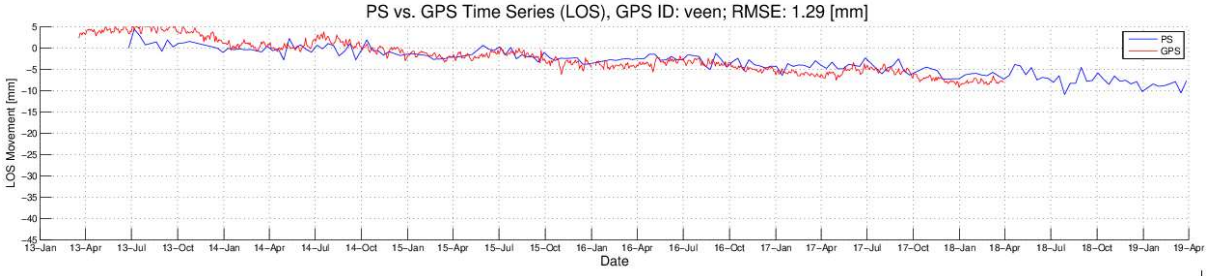
PS vs. GPS Time Series (LOS), GPS ID: veen; RMSE: 1.29 [mm]
LOS Movement [mm]
Date
PS
GPS

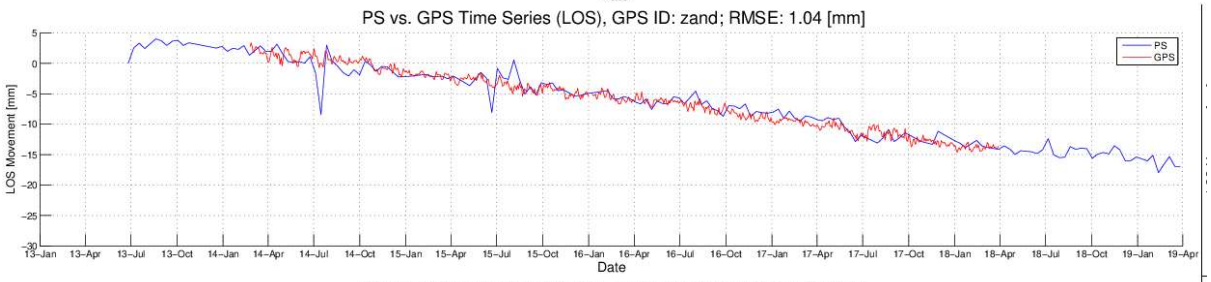
PS vs. GPS Time Series (LOS), GPS ID: zand; RMSE: 1.04 [mm]
LOS Movement [mm]
Date
PS
GPS

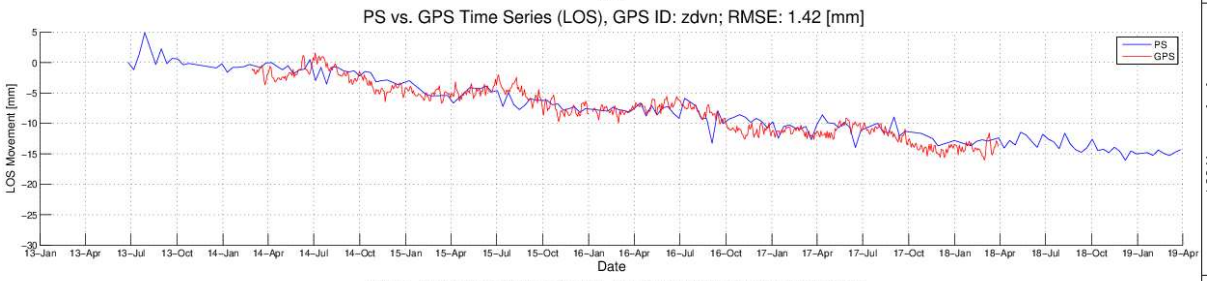
PS vs. GPS Time Series (LOS), GPS ID: zdvn; RMSE: 1.42 [mm]
LOS Movement [mm]
Date
PS
GPS

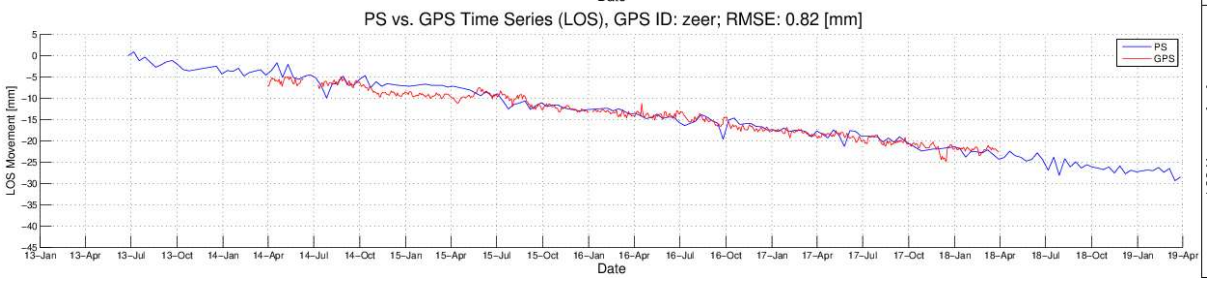
PS vs. GPS Time Series (LOS), GPS ID: zeer; RMSE: 0.82 [mm]
LOS Movement [mm]
Date
PS
GPS

Appendix B. Validation for decomposition data

B.1 Validation for velocity

B.1.1 TSX_ASC_T40 & TSX_DSC_T139

Table: Decomposition Comparison, **Vertical** Direction

GPS Name	GPS Vel. [mm/yr]	PS Vel. [mm/yr]	Difference [mm/yr]	Correlation RMSE [mm]
eems	-4.52	-4.5	0.02	0.69
froo	-4.95	-4.5	0.45	0.62
over	-4.17	-4.1	0.07	0.77
sted	-4.98	-5.5	-0.52	0.83
tenp	-5.83	-6	-0.17	1.1
usqu	-1.29	-1.3	-0.01	0.68
zand	-4.66	-4.7	-0.04	0.65
zeer	-5.47	-5.5	-0.03	0.66

Table: Decomposition Comparison, **Horizontal** Direction

GPS Name	GPS Vel. [mm/yr]	PS Vel. [mm/yr]	Difference [mm/yr]	Correlation RMSE [mm]
eems	0.81	0.5	-0.31	0.6
froo	-1.04	-0.6	0.44	0.66
over	-0.35	0	0.35	0.48
sted	0.02	0.4	0.38	0.62
tenp	-0.27	0	0.27	0.46
usqu	0.43	1.1	0.67	0.89
zand	-0.09	-0.1	-0.01	0.87
zeer	-0.49	0.1	0.59	0.72

B.1.2 TSX_ASC_T40 & TSX_DSC_T63

Table: Decomposition Comparison, **Vertical** Direction

GPS Name	GPS Vel. [mm/yr]	PS Vel. [mm/yr]	Difference [mm/yr]	Correlation RMSE [mm]
0647	-1.21	-1.5	-0.29	1.38
dzyl	-4.11	-5.1	-0.99	1.05
eems	-4.52	-4.2	0.32	0.82
froo	-4.95	-4.3	0.65	0.74
over	-4.17	-4	0.17	0.87
sted	-4.98	-5.2	-0.22	0.68
tenp	-5.83	-5.8	0.03	1.21
tjuc	-3.67	-3.5	0.17	0.78
veen	-5.12	-4.1	1.02	0.48
zand	-4.66	-4.5	0.16	0.7
zdvn	-4.05	-3.3	0.75	0.71
zeer	-5.47	-5.5	-0.03	0.83

Table: Decomposition Comparison, **Horizontal** Direction

GPS Name	GPS Vel. [mm/yr]	PS Vel. [mm/yr]	Difference [mm/yr]	Correlation RMSE [mm]
0647	-2.32	-1.1	1.22	0.95
dzyl	-0.92	-0.5	0.42	0.72
eems	0.81	0.9	0.09	0.34
froo	-1.04	-0.4	0.64	0.53
over	-0.35	0.1	0.45	0.43
sted	0.02	0.8	0.78	0.92
tenp	-0.27	0.3	0.57	0.36
tjuc	-1.16	-0.6	0.56	0.29
veen	-4.47	-4.3	0.17	0.57

zand	-0.09	0.2	0.29	0.95
zdvn	-0.37	-0.1	0.27	0.54
zeer	-0.49	0.1	0.59	0.47

B.2 Validation for decomposition time series

B.2.1 TSX_ASC_T40 & TSX_DSC_T139

B.2.1.1 Vertical

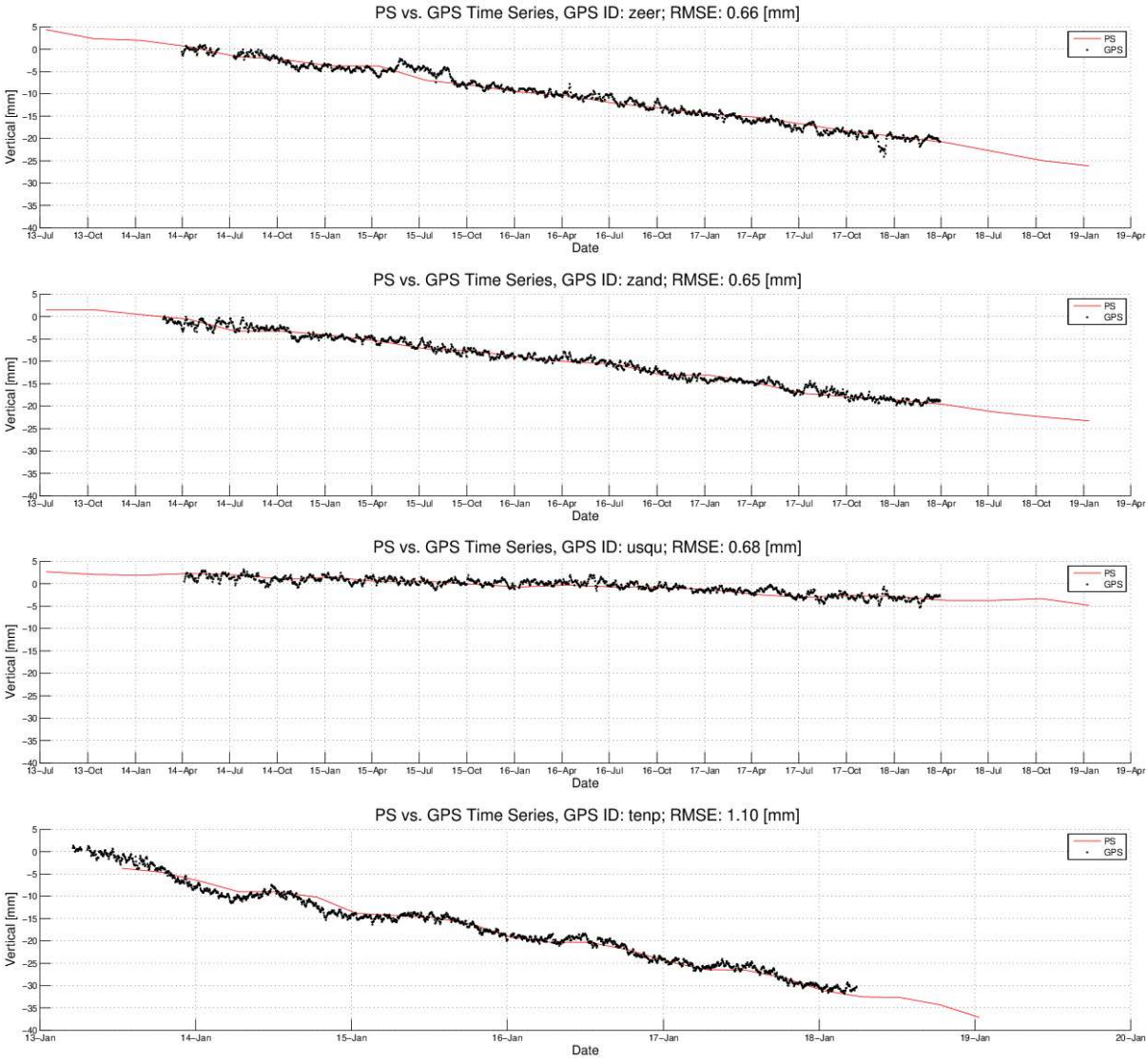

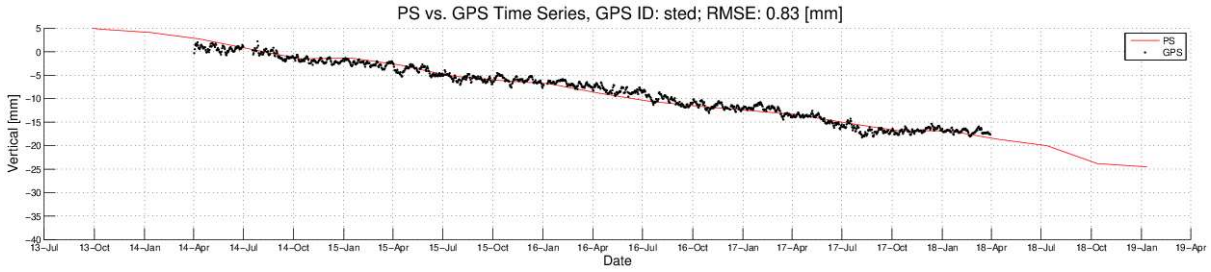

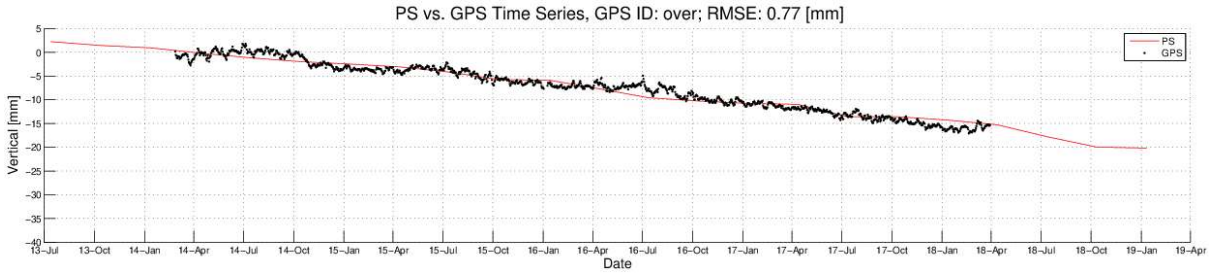

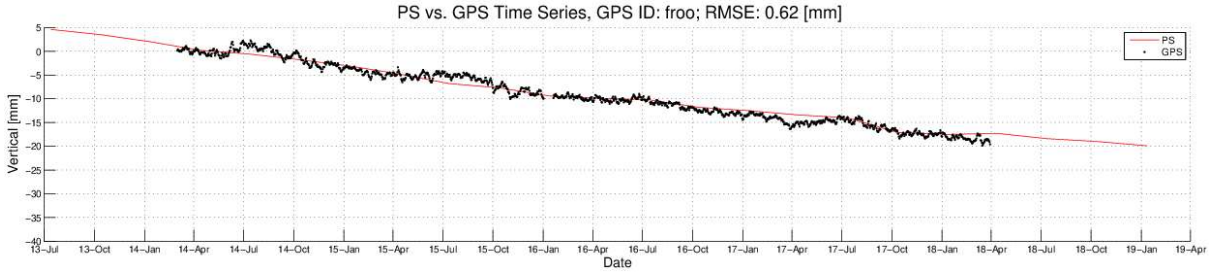

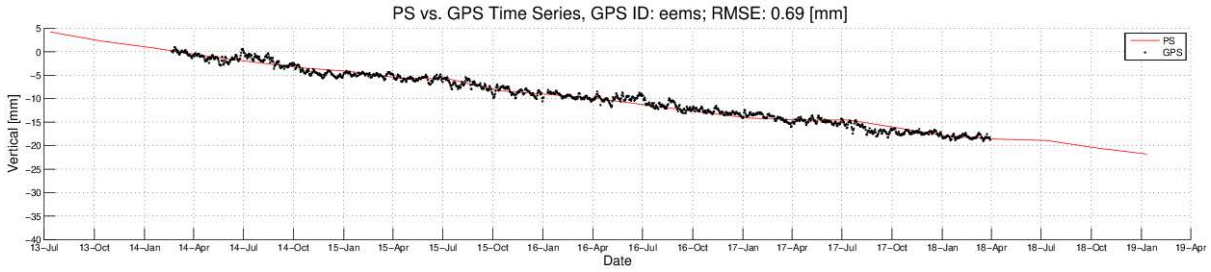

B.2.1.2 Horizontal

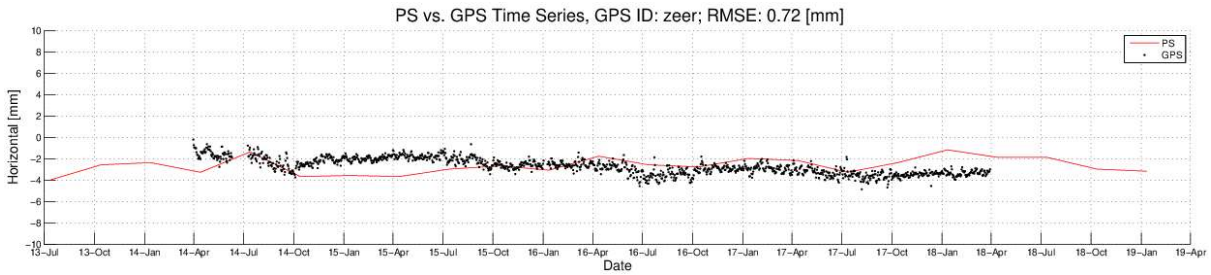

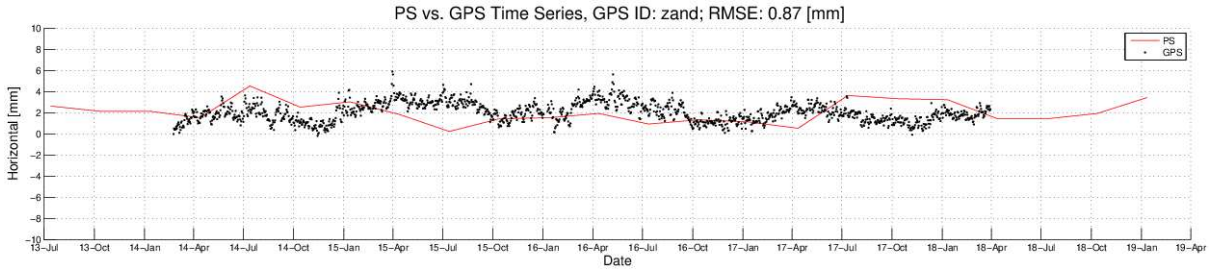

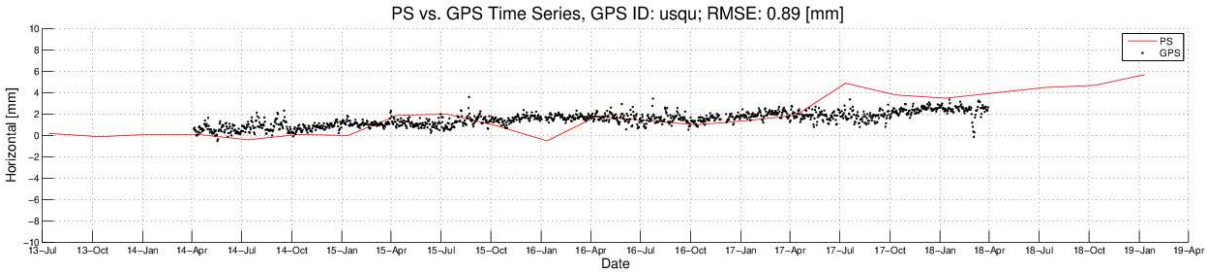
PS vs. GPS Time Series, GPS ID: usqu; RMSE: 0.89 [mm]
Horizontal [mm]
Date
PS
GPS

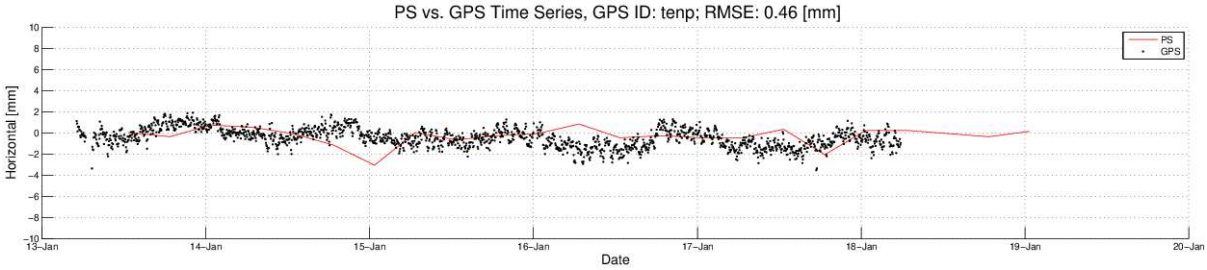
PS vs. GPS Time Series, GPS ID: tenp; RMSE: 0.46 [mm]
Horizontal [mm]
Date
PS
GPS

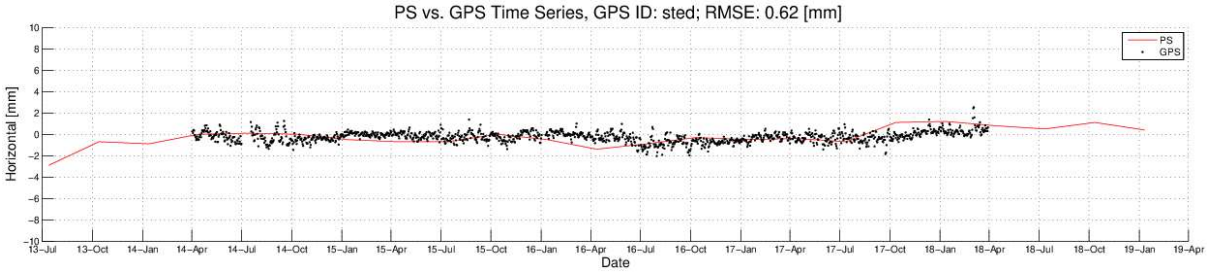
PS vs. GPS Time Series, GPS ID: sted; RMSE: 0.62 [mm]
Horizontal [mm]
Date
PS
GPS

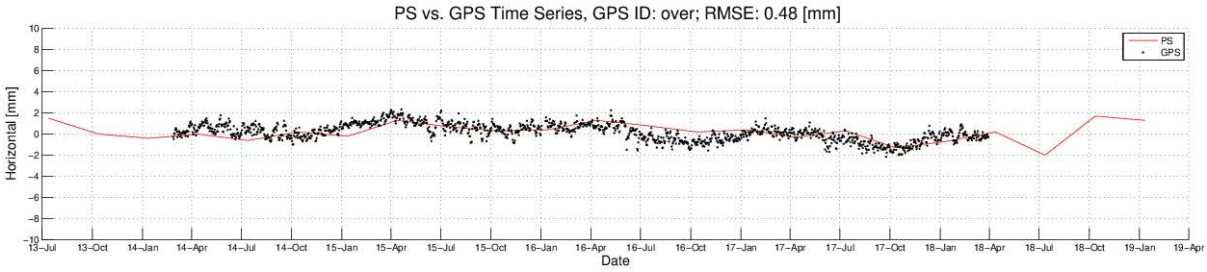
PS vs. GPS Time Series, GPS ID: over; RMSE: 0.48 [mm]
Horizontal [mm]
Date
PS
GPS

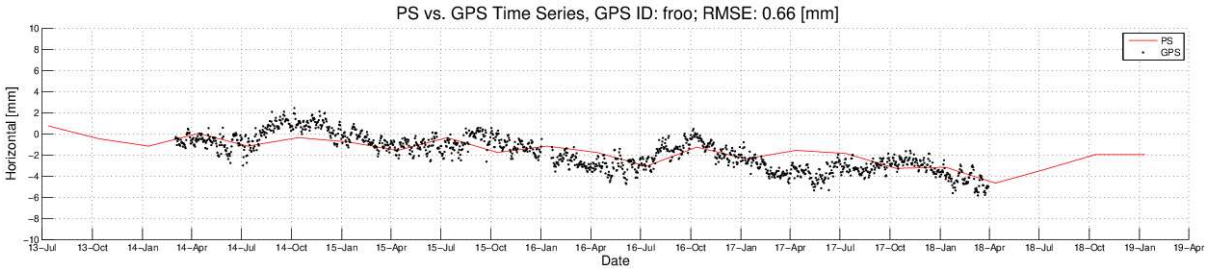
PS vs. GPS Time Series, GPS ID: froo; RMSE: 0.66 [mm]
Horizontal [mm]
Date
PS
GPS

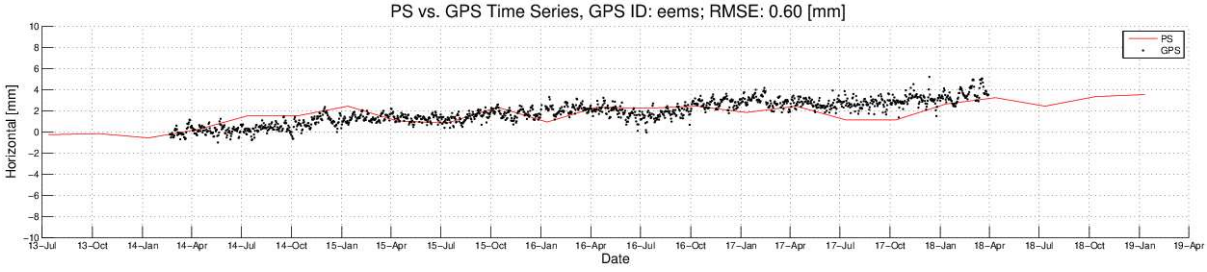
PS vs. GPS Time Series, GPS ID: eems; RMSE: 0.60 [mm]
Horizontal [mm]
Date
PS
GPS

B.2.2 TSX_ASC_T40 & TSX_DSC_T63

B.2.2.1 Vertical

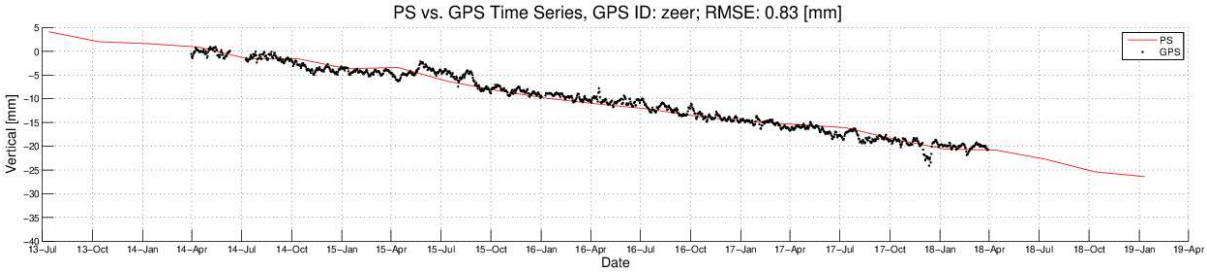

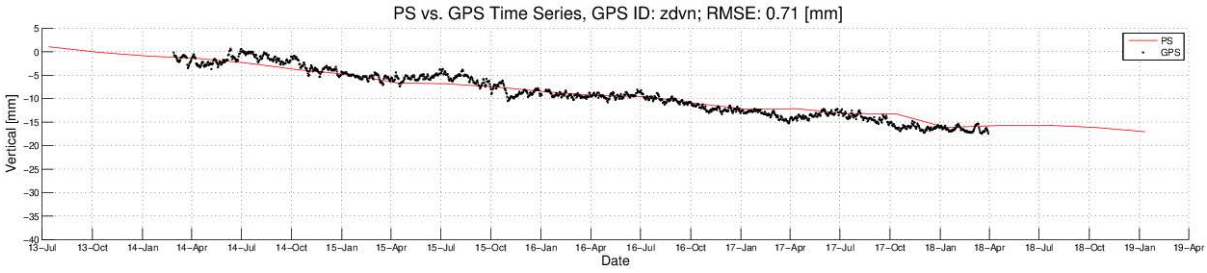

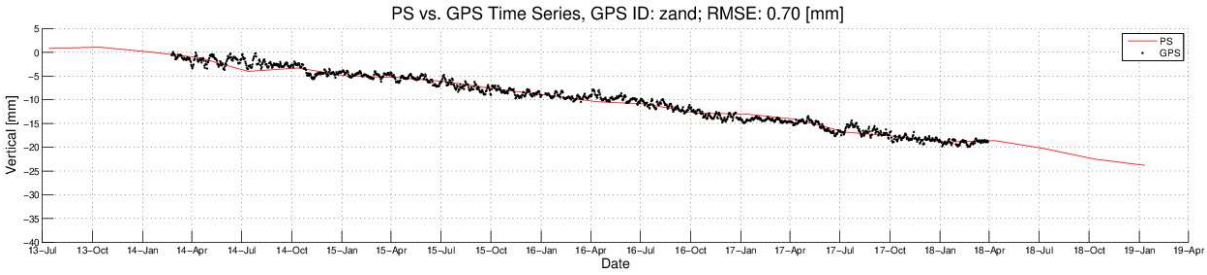

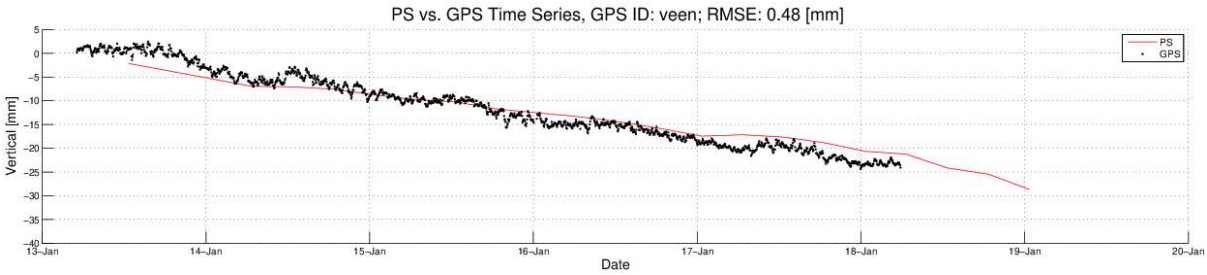

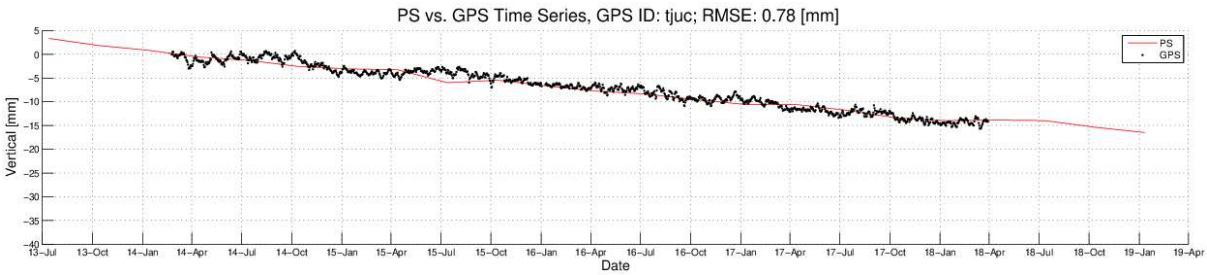

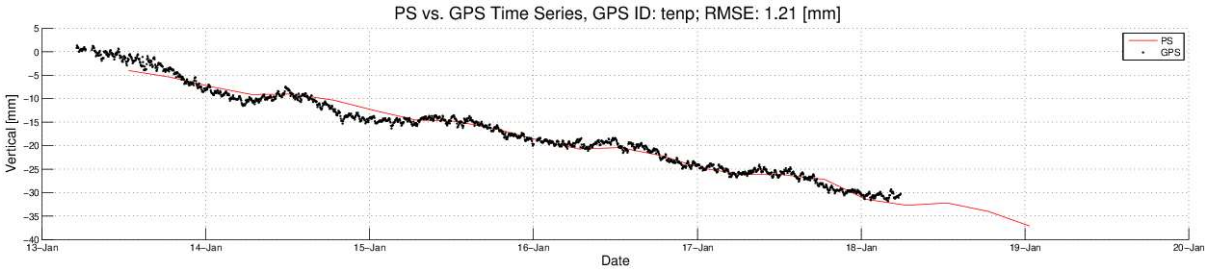
PS vs. GPS Time Series, GPS ID: tenp; RMSE: 1.21 [mm]
Vertical [mm]
Date
PS
GPS

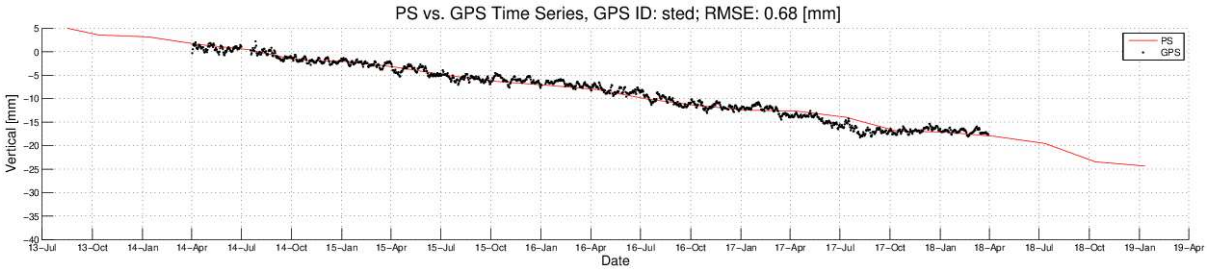
PS vs. GPS Time Series, GPS ID: sted; RMSE: 0.68 [mm]
Vertical [mm]
Date
PS
GPS

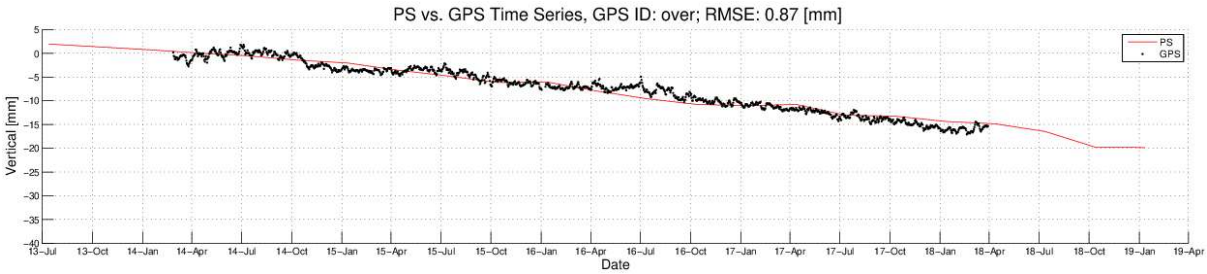
PS vs. GPS Time Series, GPS ID: over; RMSE: 0.87 [mm]
Vertical [mm]
Date
PS
GPS

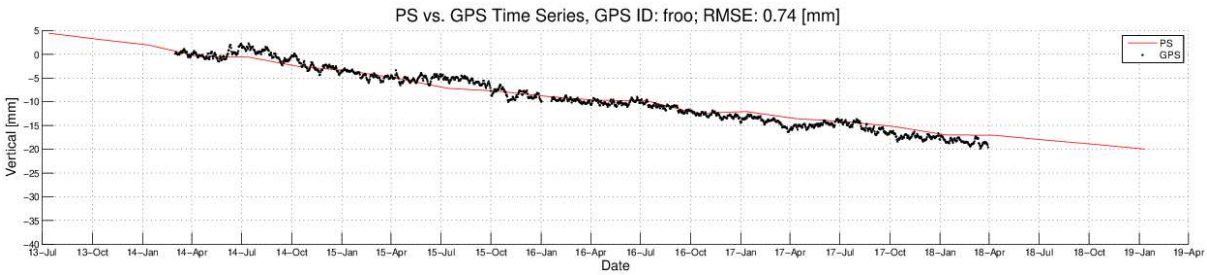
PS vs. GPS Time Series, GPS ID: froo; RMSE: 0.74 [mm]
Vertical [mm]
Date
PS
GPS

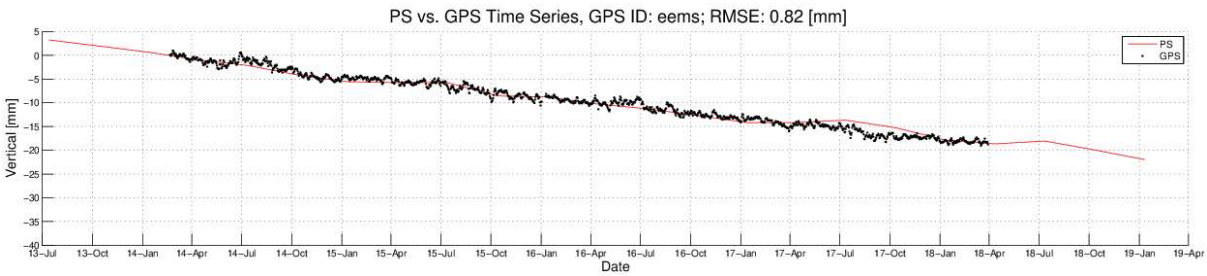
PS vs. GPS Time Series, GPS ID: eems; RMSE: 0.82 [mm]
Vertical [mm]
Date
PS
GPS

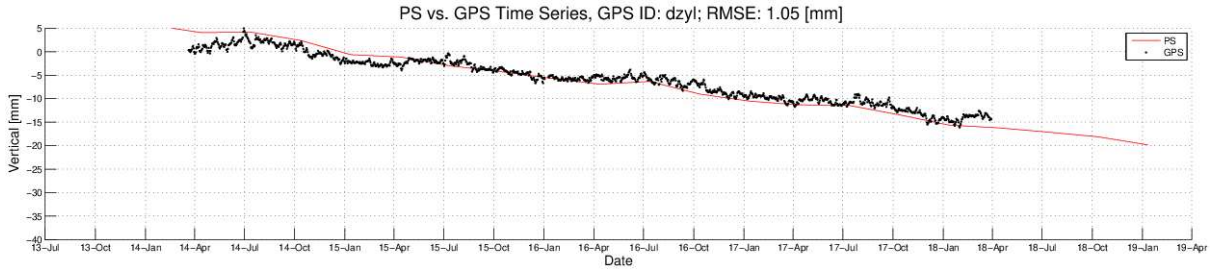

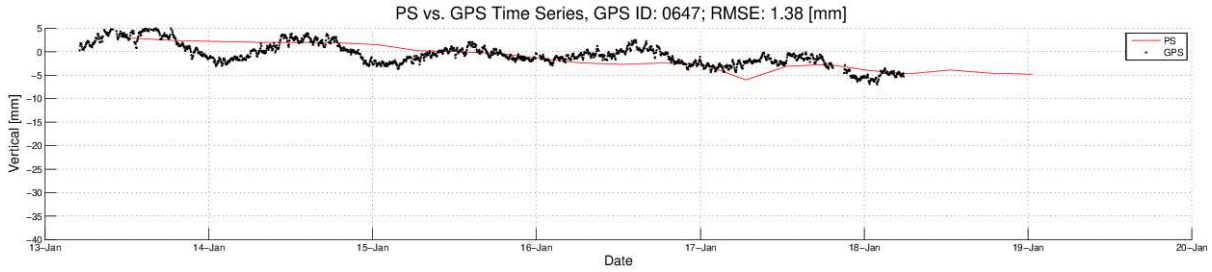

B.2.2.2 Horizontal

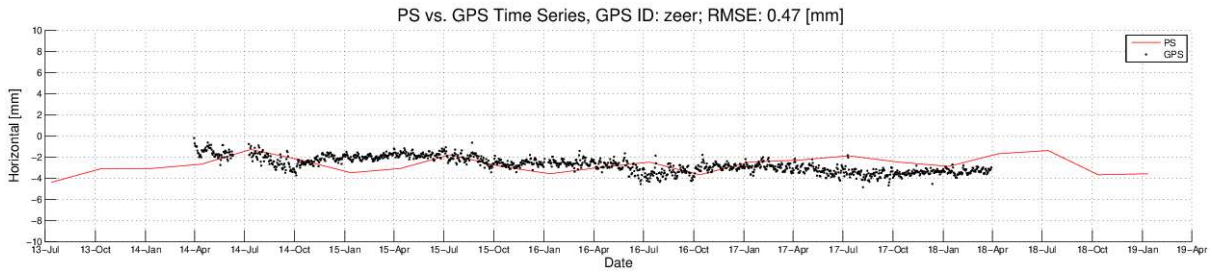

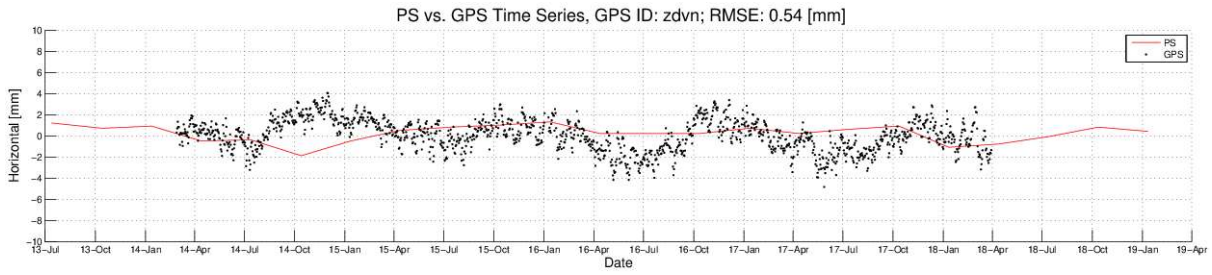

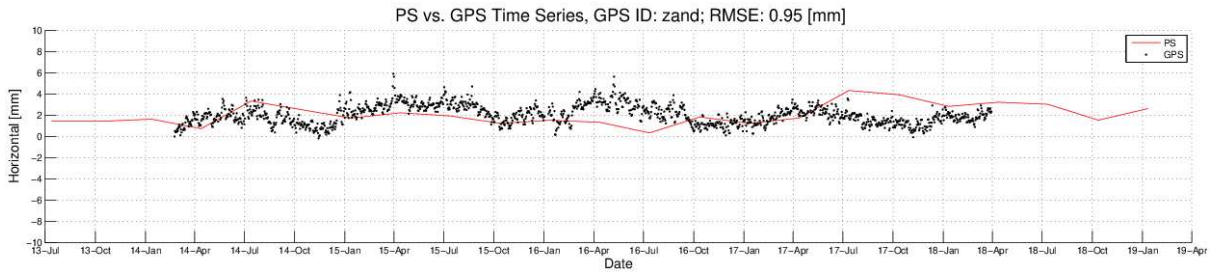

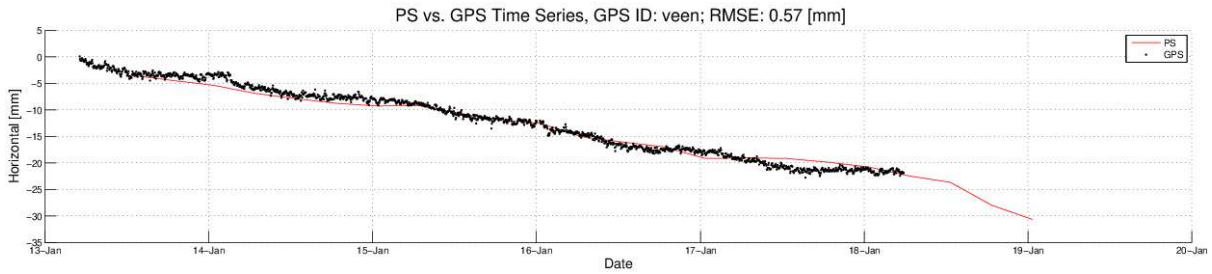

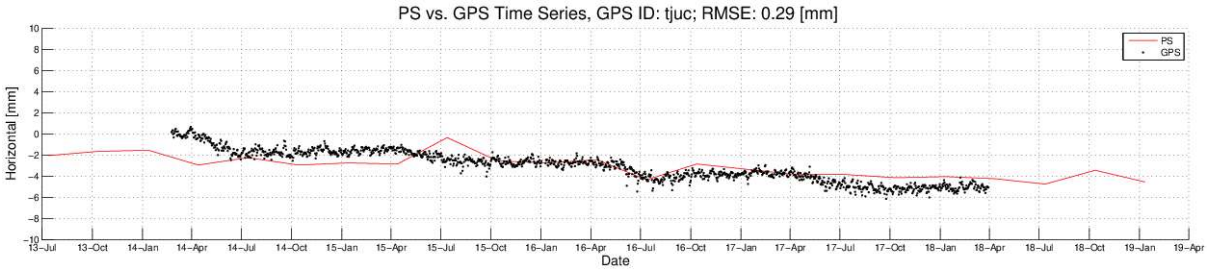
PS vs. GPS Time Series, GPS ID: tjuc; RMSE: 0.29 [mm]
Horizontal [mm]
Date
PS
GPS

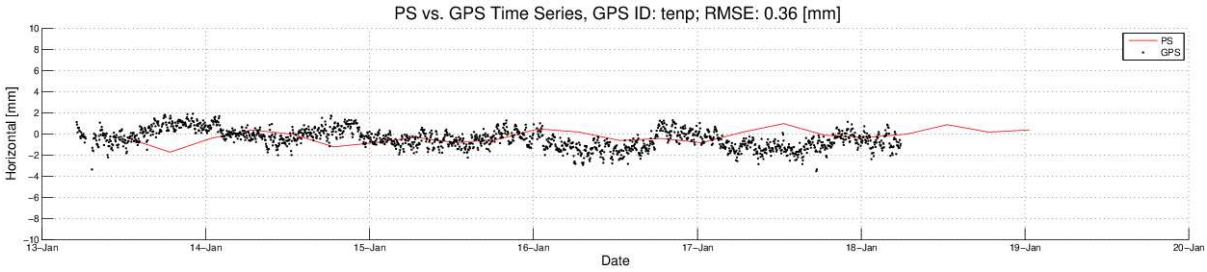
PS vs. GPS Time Series, GPS ID: tenp; RMSE: 0.36 [mm]
Horizontal [mm]
Date
PS
GPS

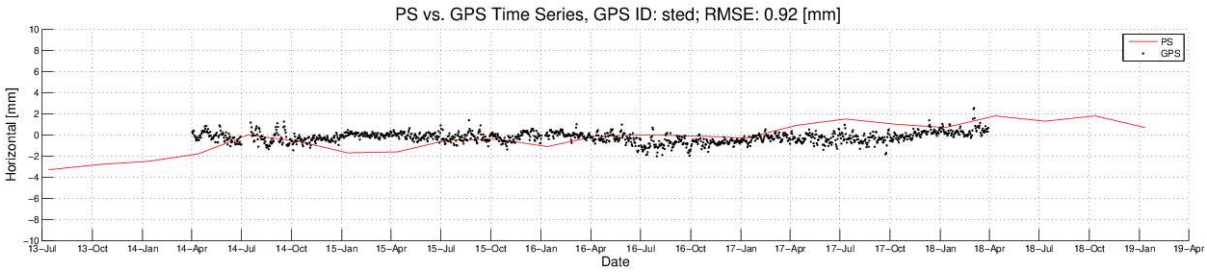
PS vs. GPS Time Series, GPS ID: sted; RMSE: 0.92 [mm]
Horizontal [mm]
Date
PS
GPS

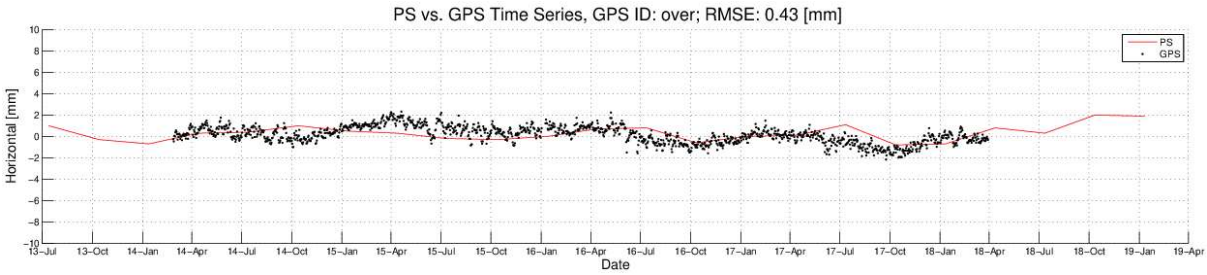
PS vs. GPS Time Series, GPS ID: over; RMSE: 0.43 [mm]
Horizontal [mm]
Date
PS
GPS

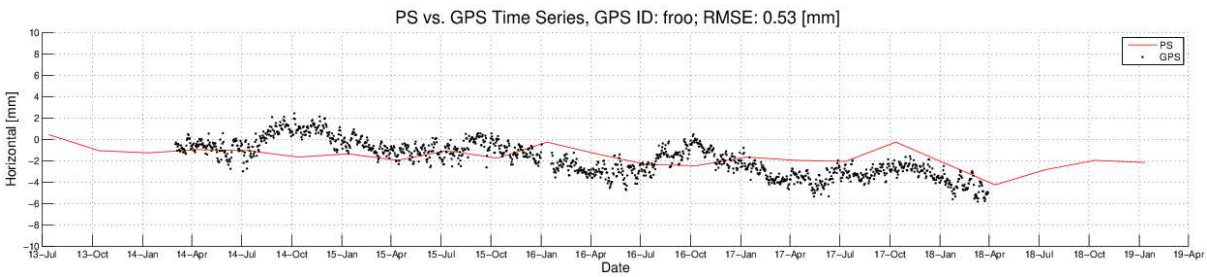
PS vs. GPS Time Series, GPS ID: froo; RMSE: 0.53 [mm]
Horizontal [mm]
Date
PS
GPS

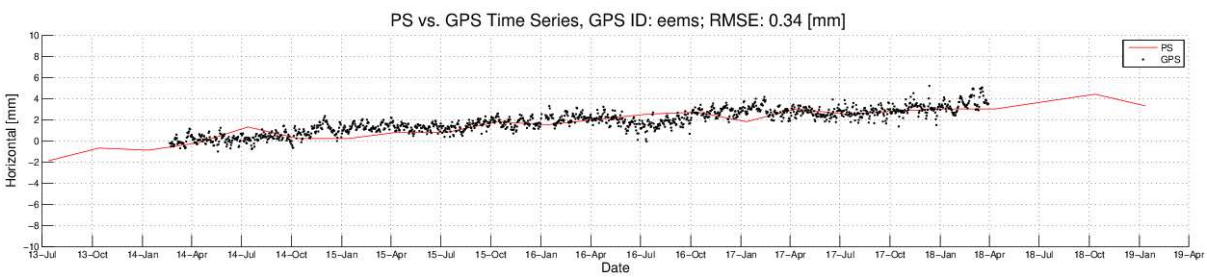
PS vs. GPS Time Series, GPS ID: eems; RMSE: 0.34 [mm]
Horizontal [mm]
Date
PS
GPS

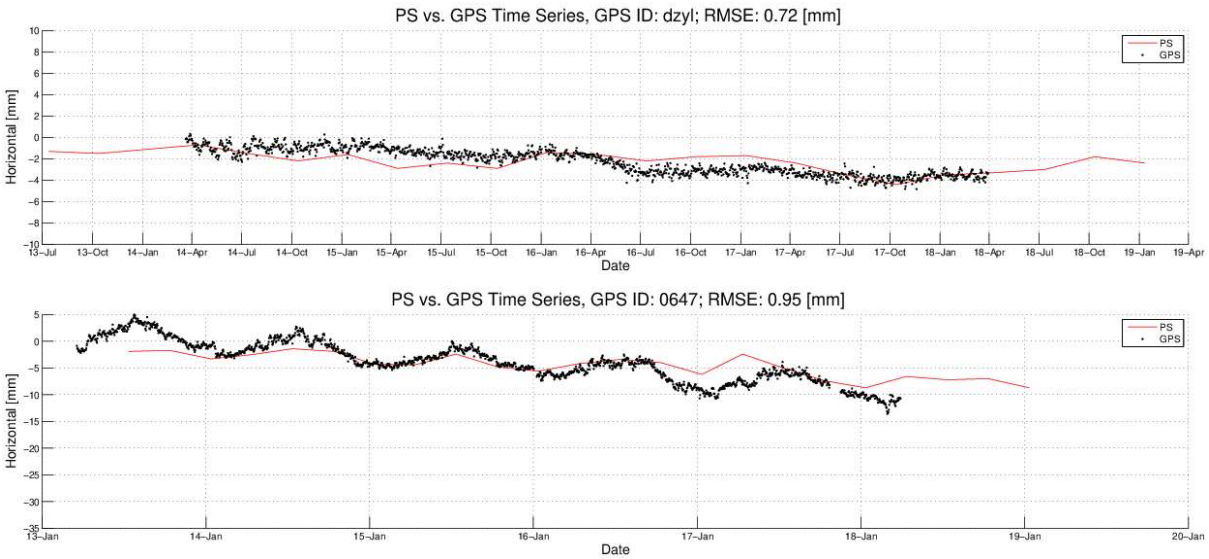
PS vs. GPS Time Series, GPS ID: dzyl; RMSE: 0.72 [mm]
Horizontal [mm]
Date
PS
GPS
PS vs. GPS Time Series, GPS ID: 0647; RMSE: 0.95 [mm]
Horizontal [mm]
Date
PS
GPS